Transient inflammatory response mediated by interleukin-1β is required for proper regeneration in zebrafish fin fold

Tomoya Hasegawa[1], Christopher J. Hall[2], Philip S. Crosier[2], Gembu Abe[3, *], Koichi Kawakami[3], Akira Kudo[1], Atsushi Kawakami[1, ‡]

[1]School of Bioscience and Biotechnology, Tokyo Institute of Technology, 4259 Nagatsuta, Midori-ku, Yokohama 226-8501, Japan

[2]Department of Molecular Medicine and Pathology, School of Medical Sciences, University of Auckland, Auckland 1023, New Zealand

[3]Division of Molecular and Developmental Biology, National Institute of Genetics, and Department of Genetics, SOKENDAI (The Graduate University for Advanced Studies), Mishima, Shizuoka 411-8540, Japan

*Present address: Laboratory of Organ Morphogenesis, Department of Developmental Biology and Neurosciences, Graduate School of Life Sciences, Tohoku University, Sendai 980-8578, Japan

‡For correspondence: atkawaka@bio.titech.ac.jp

Abstract

Cellular responses to injury are recognized to be crucial for complete tissue regeneration, but their underlying processes remain incompletely elucidated. We have previously reported that myeloid-defective zebrafish mutants display apoptosis of regenerative cells during fin fold regeneration. Here, we found that the apoptosis phenotype is induced by the prolonged expression of *interleukin 1 beta* (*il1b*). Myeloid cells have been considered to be the principal source of Il1b, but we show that epithelial cells express *il1b* in response to tissue injury and initiate the inflammatory response, and that its resolution by macrophages is necessary for the survival of regenerative cells. We further show that Il1b also plays an essential role in normal fin fold regeneration by regulating the expression of regeneration-induced genes. Our study reveals that proper levels of Il1b signaling and tissue inflammation, which are tuned by macrophages, play a crucial role in tissue regeneration.

Impact statement

The Interleukin 1 beta signaling and tissue inflammation act as a double-edged sword: they are required for regeneration, but when in excess, they impair tissue regeneration and induce apoptosis.

Introduction

Progress in regenerative medicine depends on unraveling the mechanisms underlying tissue and organ regeneration. For investigating regeneration mechanisms, zebrafish is a powerful model species because it exhibits high regenerative capacity. Zebrafish can regenerate complex structures such as fins, heart, brain, retina, and other tissues (*Gemberling et al., 2013*). The caudal fin of zebrafish, in particular, has been used as a model for analyzing epimorphic regeneration, a type of regeneration in the urodele limb and fish fin (*Poss et al., 2003*). During epimorphic regeneration, two characteristic tissues, the wound epidermis and the blastema, are induced in response to tissue amputation, and their coordinated actions regulate cell proliferation and morphogenesis and thus lead to tissue regeneration. Studies conducted using the caudal fin regeneration model have identified numerous genes and molecular signaling pathways that are critical for fin regeneration (*Yoshinari and Kawakami, 2011; Wehner and Weidinger, 2015*).

In addition to the classical regeneration model developed using the adult caudal fin, a zebrafish larval fin fold model has been developed (*Kawakami et al., 2004; Mateus et al., 2012*), and by using this model, additional genes and signaling pathways required for regeneration have been identified (*Mathew et al., 2009; Ishida et al., 2010; Yoo et al., 2012*). Specifically, the fin fold regeneration model has enabled us to adopt a genetic approach for analyzing the regeneration mechanism by exploiting a number of mutant zebrafish resources (*Rojas-Munoz et al., 2009; Yoshinari et al., 2009*), because several zebrafish lethal mutants survive beyond 7 days post fertilization (dpf)—an adequate period for assaying tissue regeneration—due to the nutrient supply from the yolk.

Previously, we reported that zebrafish mutants, *cloche* (*clo*) (*Stainier et al., 1995; Reischauer et al., 2016*) and *tal1/scl* (*Bussmann et al., 2007*), showed a unique regenerative defect: these mutants could not regenerate their fin fold due to apoptosis of the regenerative cells (*Hasegawa et al., 2015*). Our analyses of the *clo* mutant revealed that a diffusible survival factor from myeloid-lineage cells is necessary for the primed regenerative cells to avoid apoptosis. The study suggested that the regenerative cells are sensitive to apoptosis during tissue regeneration, but the mechanism of this sensitization and the identity of the survival factor remain unknown.

Myeloid cells are widely recognized to play a role in protecting against pathogens and microorganisms after tissue injury. Following tissue injury, neutrophils are first recruited to the sites of inflammation, and these cells encounter pathogens and phagocytose and kill the microorganisms by producing reactive oxygen species and/or antibacterial proteins (*Kolaczkowska and Kubes, 2013*). Subsequently, macrophages infiltrate the inflammation site, produce pro- or anti-inflammatory cytokines, remove tissue debris, secrete growth factors, and support tissue restoration (*Koh and DiPietro, 2011*).

Several recent studies have used the zebrafish model and addressed the roles of myeloid cells in response to tissue injury: Li and coworkers (*Li et al., 2012*) showed that the knockdown of macrophage differentiation delayed fin fold regeneration and resulted in the formation of an abnormal fin fold featuring large vacuoles. Furthermore, Petrie and coworkers (*Petrie et al., 2014*) showed that genetic ablation of macrophages in adult zebrafish impaired fin outgrowth and frequently induced an abnormal fin. These studies have suggested a crucial role of macrophages in tissue regeneration; however, the mechanism by which myeloid cells affect regeneration remains to be elucidated.

Here, we show that a pro-inflammatory cytokine gene, *interleukin 1 beta* (*il1b*), is aberrantly upregulated in the *clo* mutant, and that the resulting excessive and prolonged inflammation causes apoptosis of the regenerative cells. Moreover, although myeloid cells have been widely regarded as the main cells that secrete pro-inflammatory cytokines such as Il1b and thereby promote inflammation, we demonstrate that the epidermal cells that surround the amputated tissue are the source of Il1b in both wild-type (WT) and *clo* larvae. Notably, *il1b* expression in the regenerating epidermis is normally quenched by the action of macrophages, and a lack of this anti-inflammatory effect of the macrophages leads to apoptosis. Lastly, we show that Il1b signaling plays an indispensable role in normal tissue regeneration by activating the expression of regeneration-induced genes. Thus, our study highlights the function of Il1b and the inflammatory response in tissue regeneration. A proper level of *il1b* expression and the inflammatory response, which are tuned by macrophages, are necessary for the progression of tissue regeneration.

Results

Prolonged *il1b* expression in the *clo* mutant during regeneration

To understand the molecular pathway leading to the apoptosis of regenerative cells in the *clo* mutant, we performed a transcriptome analysis of amputated larval tail tissues of WT and *clo* mutant zebrafish at approximately 6 hours post amputation (hpa), right before the stage at which apoptosis first becomes detectable in the *clo* mutant (*Hasegawa et al., 2015*). As compared with WT larvae, the *clo* larvae showed a marked upregulation of regeneration-induced genes such as *junba*, *junbb*, *matrix metallopeptidase 9* (*mmp9*), *fibronectin 1b* (*fn1b*) and *fgf20a* (*Yoshinari et al., 2009; Shibata et al., 2016*) (*Figure 1A and Figure 1—figure supplement 1*). In addition to these genes, a group of genes that included *il1b* and *tumor necrosis factor-b* (*tnfb*), which are involved in the inflammatory response, also showed upregulated expression in the *clo* mutant during fin fold regeneration. Excluding enzymes and uncharacterized proteins, Il1b was the most upregulated protein. *il1b* expression in the *clo* mutant was also confirmed using reverse transcription polymerase chain reaction (RT-PCR) analysis (*Figure 1B*). Notably, *prostaglandin2a* (*ptgs2a*), a downstream gene in Il1b signaling (*Dinarello, 2009*), was also upregulated in the *clo* mutant (*Figure 1A*), which clearly indicated that Il1b signaling was activated in the *clo* mutant.

Next, we performed *in situ* hybridization (ISH) analysis of *il1b* to reveal its spatiotemporal expression during regeneration. At 3 hpa, strong *il1b* expression was observed in both WT and *clo* mutant larvae (*Figure 1C and D*). In WT larvae, *il1b* was expressed in a group of scattered cells that appeared to be myeloid cells (*Figure 1C*; arrowheads) and also expressed in the distal edge of the fin fold. After 3 hpa, *il1b* expression was rapidly diminished in WT larvae, and most larvae displayed very weak or no *il1b* expression at 6 hpa. In contrast to the expression in WT, *il1b* expression in the *clo* mutant was maintained at 6 hpa and, furthermore, detectable at 12 hpa, which indicated that a prolonged inflammatory reaction occurs in the *clo* mutant.

Bacterial infection is recognized to trigger an inflammatory response that accompanies the induction of *il1b* expression (*Dinarello, 2009*). To investigate whether the same mechanism underlies the induction of *il1b* expression by fin fold amputation and bacterial infection, we injected

zebrafish with *Salmonella typhosa* lipopolysaccharide (LPS), a reagent whose injection mimics bacterial infection (*Lu et al., 2008*). WT larvae injected with LPS displayed systemic induction of *il1b* in cells that appeared to be myeloid cells (*Figure 1E*). By contrast, the *clo* mutant larvae injected with LPS showed few *il1b*-positive cells, which indicated that tissue injury and bacterial infection induce *il1b* expression through distinct mechanisms.

_il1b_ is expressed in epithelial cells during fin fold regeneration

The absence of myeloid cells and the expression of *il1b* in the *clo* mutant suggested that *il1b* is expressed in non-myeloid cells in the *clo* mutant. Accordingly, examination of tissue cryosections of the *clo* fin fold after *il1b* ISH analysis suggested that *il1b* was expressed in epidermal cells (*Figure 2A*).

To further investigate the identity of the *il1b*-expressing cells, we generated a transgenic (Tg) line, Tg(*il1b*:*egfp*), by introducing the *egfp-nitroreductase* fusion gene into the *il1b* locus of a bacterial artificial chromosome (BAC) clone, CH211-147H23. The larvae of Tg(*il1b*:*egfp*) showed faint EGFP expression in the entire epidermis and weak EGFP expression in pectoral fins and at the end of the notochord (*Figure 2—figure supplement 1A*; arrowheads). After fin fold amputation, *egfp* expression was induced in a similar pattern as endogenous *il1b* expression (*Figure 2B; Figure 2—figure supplement 1B*), although EGFP fluorescence was detected at later stages of regeneration than *il1b* mRNA, probably due to the relatively longer half-life of the protein EGFP. Furthermore, LPS injection also induced EGFP fluorescence in myeloid cells (*Figure 2—figure supplement 1C*), which indicated that the *il1b:egfp* transgene recapitulated endogenous *il1b* expression in myeloid cells and also in the injured fin fold.

Next, by using the Tg(*il1b*:*egfp*) reporter line, we confirmed that the EGFP-positive cells in the transgenic line mostly colocalized with the epithelial marker E-cadherin (*Figure 2C*), in both WT and the *clo* mutant; this finding indicated that *il1b* expression was principally induced in epithelial cells in response to tissue amputation. In addition to detecting *il1b* expression in the injured tissue, we detected *il1b* expression in WT larvae in migrating cells that are likely to be the myeloid cells

(*Video 1*). Thus, our results demonstrated that the epidermal cells that surround the site of injury are the source of Il1b, and that myeloid cells exert a suppressive effect on *il1b* expression.

Il1b signaling and inflammation are responsible for apoptosis in the *clo* mutant

Excessive inflammation has been suggested to directly or indirectly induce apoptosis (*Wallach et al., 2014*). Specifically, because elevated expression of the pro-inflammatory cytokine Il1b leads to chronic inflammation (*Dinarello, 2011*), we suspected that excessive *il1b* expression in the *clo* mutant could be a cause of the apoptosis of regenerative cells.

First, we used the Tg(*il1b:egfp*) reporter line to examine the relationship between *il1b*-expressing cells and apoptotic cells. Although many of the *il1b*-expressing cells did not overlap with the apoptotic cells that were mainly distributed in the mesenchyme (*Hasegawa et al., 2015*), the apoptotic cells lay in close apposition to the *il1b*-expressing cells (*Figure 3A*).

Next, to demonstrate the role of Il1b in the apoptosis occurring in the *clo* mutant, we knocked down *il1b* expression using an antisense morpholino oligonucleotide (MO). The *il1b* MO1 targeted to the splice sites (*Nguyen-Chi et al., 2014*) effectively inhibited *il1b* mRNA splicing (*Figure 3B*). Notably, *il1b* knockdown in the *clo* mutant resulted in a reduction in the apoptosis of regenerative cells, whereas in the *clo* mutant injected with the standard control MO (std MO), no reduction in apoptosis was detected (*Figure 3C and D*). A similar anti-apoptosis effect of *il1b* knockdown was also obtained by using another MO against *il1b* (*Yan et al., 2014*) (*Figure 3—figure supplement 1*).

To examine whether excessive inflammation is a cause of the apoptosis in the *clo* mutant, we used dexamethasone (Dex), a synthetic glucocorticoid that has been reported to suppress inflammation and *il1b* expression (*Kern et al., 1988*). Our results showed that Dex treatment abolished *il1b* expression in the *clo* mutant starting from an early stage of regeneration (*Figure 3E*), which indicated that the treatment effectively suppressed inflammation and *il1b* expression. In the Dex-treated *clo* larvae, the apoptosis of regenerative cells was rescued, much as it was in the *il1b*-knockdown larvae (*Figure 3F and G*). Collectively, these data support the notion that excessive Il1b signaling and inflammation in response to tissue injury represent a cause of apoptosis in the *clo*

mutant.

Macrophages support the survival of regenerative cells

We have previously shown that the presence of myeloid cells is essential for the survival of regenerative cells (*Hasegawa et al., 2015*). The myeloid cells such as the neutrophils and macrophages have been shown to transiently migrate to the injured fin fold (*Li et al., 2012*). Actually, we observed that the myeloid cell accumulation in the injured fin fold reached at a maximum number between 3 – 6 hpa (*Figure 4A and B)*. The timing coincides with the stage when the initial *il1b* expression immediately after wounding was downregulated (*Figure 1C and D*). This suggests a possibility that myeloid cell migration could play a role for attenuating *il1b* expression, although we cannot conclude that the myeloid cell migration is necessary for *il1b* downregulation.

Myeloid cells comprise several different cell types, including neutrophils and macrophages, but the cell type that is required for the survival of regenerative cells remains to be determined. Here, we used *csf3r*, *irf8*, and *spi1b* (*pu.1*) MOs, which inhibited the differentiation of neutrophils, macrophages, and both types of cells, respectively, and examined whether the depletion of neutrophils or macrophages induces the apoptosis of regenerative cells as in the *clo* mutant. The efficacy of *csf3r* knockdown was confirmed by the Sudan Black staining of neutrophils and the ISH analysis using the *mpx* probe. In both the *csf3r* morphants and the *spi1b* morphants, fewer neutrophils were detected than in the control morphants (*Figure 4—figure supplement 1A, B, D*). In the *irf8* morphants, the expression of *apoeb*, a marker for microglia—the resident macrophages in the central nervous system—was drastically decreased (*Figure 4—figure supplement 1C*). The decrease of macrophages was also evident in the wounded fin fold as revealed by the *lcp1* ISH analysis (*Figure 4—figure supplement 1E*). None of these morphants showed any morphological abnormalities. These data indicated that the *irf8* MO effectively inhibited macrophage differentiation.

To examine apoptosis, we performed the TUNEL staining in the aforementioned morphants after fin fold amputation, and the results showed that *irf8* morphants exhibited aberrant apoptosis of the

207 regenerative cells, as in the case of the *spi1b* morphants (*Hasegawa et al., 2015*) (*Figure 4C*).
208 Importantly, similar numbers of TUNEL-positive cells were observed in the *irf8* and the *spi1b*
209 morphants (*Figure 4D*). In sharp contrast to the *irf8* morphants, the *csf3r* morphants showed no
210 increase in the apoptosis of regenerative cells. These results suggest that macrophages are
211 responsible for supporting the survival of regenerative cells.
212
213 **Macrophages attenuate *il1b* expression and inflammation**
214 We next investigated the mechanism by which macrophages support the survival of regenerative
215 cells. First, we examined *il1b* expression at 6 hpa in the *spi1b*, *csf3r*, and *irf8* morphants. Whereas
216 normal *il1b* expression was detected in the *csf3r* morphants, as in WT larvae, *il1b* expression
217 remained elevated in the *spi1b* and *irf8* morphants, as in the *clo* mutant (*Figure 5A and B*). The result
218 suggested that macrophages attenuated *il1b* expression and thereby prevented the apoptosis of
219 regenerative cells in WT larvae. Furthermore, the apoptosis induced in the *spi1b* or *irf8* morphants
220 was rescued following *il1b* knockdown or Dex treatment (*Figure 5C–E*), which suggested that
221 elevated Il1b expression in the *spi1b* and *irf8* morphants is responsible for the observed apoptosis.
222
223 **Il1b overexpression induces aberrant apoptosis and thereby suppresses fin fold regeneration**
224 To further demonstrate that excessive *il1b* expression induces apoptosis, we generated and used the
225 construct pTol2(*hsp70l:mCherry-T2a-il1b*), which we hereafter refer to as pTol2(*hsp70l:il1b*). The
226 precise cleavage site of the zebrafish Il1b pro-peptide has not yet been identified (*Vojtech et al.,*
227 *2012*), but based on comparing the zebrafish and human sequences, we estimated that the human
228 IL-1β cleavage site (D116) corresponds to the threonine residue at the 124th amino acid (a.a.)
229 position in zebrafish Il1b (*Figure 6—figure supplement 1A*). Furthermore, to obtain constitutive
230 secretion of this Il1b protein lacking a canonical signal-peptide sequence, the Il1b sequence after a.a.
231 125 was fused with the human IL-1β receptor antagonist signal sequence (*Wingren et al., 1996; Tu et*
232 *al., 2008*) and placed under the control of the promoter of *heat shock protein 70l* (*Figure 6A*). In the
233 obtained Tg(*hsp70l:il1b*) line, mCherry fluorescence and *il1b* expression were observed after heat

234 shock treatment (*Figure 6B; —figure supplement 1B*), but not by a stress caused by fin fold
235 amputation (*Figure 6—figure supplement 1C*).
236 When TUNEL staining was performed after heat shock induction at 2 days post amputation (dpa),
237 several TUNEL-positive cells were detected in the injured fin fold (*Figure 6C and D*), which
238 indicated that the primed regenerative cells were susceptible to the excess Il1b signal. Furthermore, a
239 systemic and aberrant apoptosis was also observed when *il1b* was overexpressed in WT embryo
240 from 12 – 24 hours post fertilization (hpf), at which stage myeloid cells have not fully differentiated
241 (*Figure 6—figure supplement 1D*). This clearly indicated that the excessive Il1b signaling potentially
242 induces apoptosis not only in fin fold but also in other parts of the body. In addition to inducing the
243 aberrant apoptosis, *il1b* overexpression suppressed the extension of the fin fold (*Figure 6E and F*).
244
245 **Normal inflammation mediated by Il1b is required for fin fold regeneration**
246 Our data thus far suggested that excessive Il1b-mediated inflammation negatively affects the
247 survival of regenerative cells and tissue regeneration in the *clo* mutant. However, inflammation has
248 also been suggested to be essential for complete tissue regeneration (*Mathew et al., 2007; King et al.,*
249 *2012; Kyritsis et al., 2012*). To examine the role of tissue inflammation and Il1b during normal fin
250 fold regeneration, we used Dex and *il1b* MO1 and tested whether the inflammation mediated by Il1b
251 affects normal fin fold regeneration.
252 To assess the role of inflammation in tissue regeneration, we administered Dex to WT larvae
253 and assessed fin fold regeneration. The Dex-treated larvae displayed an apparent retardation of
254 regeneration at 3 dpa (*Figure 7A and B*) and a statistically significant reduction in cell proliferation
255 in the distal fin fold region (*Figure 7C and D*). Notably, the expression of regeneration-induced
256 genes such as *junba* (*Yoshinari et al., 2009*) and *fgf20a* (*Whitehead et al., 2005; Shibata et al., 2016*)
257 was downregulated in the Dex-treated larvae (*Figure 7E*). These data suggested that inflammation is
258 required for the activation of regeneration-induced gene expression and regeneration.
259 Next, we used *il1b* knockdown in WT zebrafish to demonstrate the role of Il1b signaling in
260 normal regeneration: *il1b* knockdown induced a similar phenotype as Dex treatment (*Figure 7F–I*),

although the phenotype was slightly milder than that of the Dex-treated larvae, probably due to the lower penetrance of the MO knockdown. Importantly, similar to the Dex-treated larvae, the *il1b* morphants showed attenuated expression of *junba* and *fgf20a* (*Figure 7J)*. Collectively, these results suggest that the inflammatory reaction mediated by Il1b plays a necessary role in normal fin fold regeneration.

Lastly, we tested whether *il1b* overexpression induces a marked increase in the expression of the regeneration-induced genes *junba*, *junbb* and *fn1b* in uninjured tissue (*Figure 7K*). As per our expectation, *il1b* overexpression induced the ectopic expression of *fn1b*, *junba*, and *junbb* both in the uncut fin fold (*Figure 7L*) and in several other tissues such as the pectoral fins. Importantly, the apoptosis induced by *il1b* overexpression was only detectable at 2 days after multiple heat shocks (*Figure 6C and D*), which is possibly due to the anti-inflammatory function of macrophages in WT. But, the induction of *junba*, *junbb* and *fn1b* was observed at 12 hours after two heat shocks, a stage when the apoptosis induced by *il1b* overexpression has not taken place (*Figure 7—figure supplement 1*), indicating that the expression of the regeneration-induced genes was not due to an indirect regenerative response to cell death. These data indicated that Il1b signaling is required for stimulating the expression of regeneration-induced genes and regulating the initiation of fin fold regeneration.

Discussion

Myeloid cells have been suggested to play crucial roles in the inflammatory responses of injured tissues. The pro-inflammatory cytokines (such as Il1b) that are produced by myeloid cells, including macrophages, induce the early response against infection or injury (*Dinarello, 2009*). Thus, myeloid cells are considered to trigger inflammation by providing pro-inflammatory cytokines. Here, we demonstrated that the pro-inflammatory cytokine Il1b is provided by epidermal cells in response to tissue injury. We showed that apoptosis occurred if the Il1b action at the injury site was prolonged, and that macrophages were responsible for the attenuation of *il1b* expression and resolution of the inflammation. Furthermore, our data suggested that normal Il1b expression and inflammatory

response play a necessary role in tissue regeneration by activating the expression of regeneration-induced genes. Thus, our study has revealed that Il1b signaling and tissue inflammation act as a double-edged sword: they are required for regeneration, but when in excess, they impair tissue regeneration (*Figure 8*).

Myeloid cells have been considered to be the principal producers of Il1b, although certain studies have reported *il1b* expression in melanoma cells (*Okamoto et al., 2010*) and human keratinocytes (*Kupper et al., 1986*). In this study, we showed that *il1b* is expressed by the epidermal cells present around the injury site. Notably, LPS injection induced *il1b* expression in myeloid cells, but not in the injured epidermal cells; this finding suggests that *il1b* induction by tissue injury occurs through a mechanism that is distinct from the mechanism underlying the induction in myeloid cells following bacterial infection. Although how tissue injury stimulates *il1b* expression remains unknown and is a subject for future study, a substance released from disrupted cells (*Rock and Kono, 2008*) or a mechanical signal could be responsible for inducing *il1b* expression (*Kanjanamekanant et al., 2013*).

We also showed here that in the *clo* mutant, apoptosis is caused by prolonged *il1b* expression and inflammatory response. The precise mechanism by which Il1b induces apoptosis is unclear, but Tnf signaling could be a downstream mediator for triggering apoptosis. Tnfα signaling is known to stimulate apoptosis through the activation of Caspase 8 (*Sedger and McDermott, 2014*). Tissue inflammation has been suggested to induce *tnfα* expression, and zebrafish *tnfb*, one of the zebrafish homologs of *tnfα*, was upregulated in the *clo* mutant (*Figure 1A*); therefore, Tnfα signaling could potentially serve as a direct mediator for inducing apoptosis in the *clo* mutant. Alternatively, the *clo* apoptosis might occur due to ER stress signaling: Il1b administration into primary rat β-cells and MIN6 cells was reported to increase ER stress through intracellular release of Ca^{2+} and induce apoptosis in a JNK-dependent manner (*Eizirik and Mandrup-Poulsen, 2001; Wang et al., 2009*). Thus, excessive ER stress evoked by Il1b around the injury site could induce apoptosis in the *clo* mutant.

In this study, we further demonstrated that macrophages play a crucial role in fin fold regeneration by attenuating the *il1b* expression and supporting survival of the regenerative cells.

315 Recent studies have shown that the knockdown of macrophage differentiation delayed fin fold
316 regeneration and result in an abnormal fin fold featuring large vacuoles (*Li et al., 2012*), and genetic
317 ablation of macrophages in adult zebrafish was demonstrated to affect fin ray patterning and fin
318 growth (*Petrie et al., 2014*). These studies suggested that macrophages play a critical role in tissue
319 regeneration, but the precise function of the cells has remained unknown. Our study has, for the first
320 time, elucidated a role of macrophages in attenuating Il1b expression and inflammation during tissue
321 regeneration. In accord with our observation, macrophage-depleted mice and salamanders were
322 found to display elevated *il1b* expression (*Goren et al., 2009; Godwin et al., 2013*), which suggests
323 that the macrophage function of attenuating *il1b* transcription is conserved in other vertebrate
324 species.

325 Our observation of macrophage accumulation in the injured fin fold suggested that the
326 macrophage migration could play a role for attenuating the *il1b* expression and quenching
327 inflammation. However, we cannot conclude that the macrophage migration is necessary for
328 attenuating the *il1b* expression, because our preceding study has shown that an activity that rescues
329 the *clo* apoptosis exists in the WT body extract prior to tissue amputation. We previously suggested
330 that the effect of myeloid cells is mediated by a factor that is diffusible and heat-stable (*Hasegawa et*
331 *al., 2015*), but its identity remains unknown. The factor could be an anti-inflammatory
332 protein/molecule such as IL-10, Tgf-β, or a lipid mediator (*Serhan et al., 2008; Ortega-Gómez et al.,*
333 *2013*). It is speculated that signals like the nFkB and/or STAT3 that are activated by tissue injury are
334 involved in inducing the *il1b* expression (*Fang et al., 2013; Ogryzko et al., 2014; Karra et al., 2015*).
335 The anti-inflammatory molecules bind to cell surface receptors to activate intracellular pathways and
336 antagonize the nFkB and/or STAT3 signals to attenuate the *il1b* transcription (*Yu et al., 2009;*
337 *Saraiva and O'Garra, 2010; Liao et al,. 2012*).

338 Most importantly, our study suggests that inflammation mediated by Il1b is also necessary for
339 proper fin regeneration. Previously, we showed that genes such as *fn1b*, *junba*, and *junbb* were
340 induced in response to tissue injury (*Yoshinari et al., 2009*), but the upstream mechanism that
341 regulates the expression of these genes has remained unknown. Here, we have demonstrated that

Il1b signaling is necessary and sufficient for triggering the expression of regeneration-induced genes. Although the primary factors involved in tissue regeneration, tentatively named alarmins (*Bianchi, 2007*), remain to be identified, Il1b could represent one of the key upstream mediators for initiating the expression of regeneration-induced genes and advancing tissue regeneration.

Given that macrophages are required for resolving inflammation, an impairment or reduction of this function will lead to the diseases that accompany chronic inflammation, such as rheumatoid arthritis, inflammatory bowel disease, and auto-inflammatory diseases. Therefore, elucidation of the regulatory mechanism of the Il1b signal and the action of anti-inflammatory substances released from macrophages will enhance our understanding of the pathogenic processes of chronic-inflammation diseases and lead to the development of suitable therapeutics.

Materials and methods

Fish husbandry and fin amputation

Zebrafish of a WT line, which has been maintained in our facility for >10 years through inbreeding, were housed in a recirculating system in a 14-h day/10-h night cycle at 28.5°C. When necessary, larvae were incubated in egg water (0.06% artificial marine salt, 0.0002% methylene blue) containing 0.003% phenylthiourea to prevent pigment formation. The zebrafish mutant strain *clo*^{m39} (RRID:ZFIN_ZDB-ALT-980203-381), the *fgf20a* enhancer-trap line *HGn21A* (*Shibata et al., 2016*), the BAC Tg(*il1b*:*egfp*) line, and Tg(*hsp70l:il1b*) were used. The *clo*^{m39} mutant was genotyped as previously described (*Hasegawa et al., 2015*). Zebrafish were subject to heat-shock induction at 38°C for 1 h in a small water bath and then cooled to 28.5°C over time. Fin fold fin amputation was performed as previously described (*Kawakami et al., 2004*). Briefly, zebrafish larvae at 2 dpf were anesthetized with 0.04% 3-amino benzoic acid ethylester (tricaine) in egg water and amputated their fin fold with a surgical razor blade. For reproducible quantification, fin fold was carefully amputated at sites just posterior to the notochords. For quantification of fin fold regeneration in *Figure 6F*, *Figure 7B and 7G*, the length from the notochord end to the posterior tip of fin fold was measured.

RNA sequencing analysis

Larval posterior tissues (~1 mm from the distal end, approximately the tissue posterior to the yolk extension) from uncut WT, amputated WT, and amputated *clo* mutant, which were obtained from >5 independent batches of incrosses of *clo* heterozygotes, were collected on dry ice and stored at −80°C. Total RNAs from approximately 500 posterior tissue samples were extracted by using TRIzol (Thermo Fisher Scientific, Waltham, MA) according to the manufacturer's instructions. RNA sequencing analysis was performed by Dragon Genomics (Kyoto, Japan). Briefly, purified and fragmented PolyA$^+$ RNAs were prepared from 3 μg each of the total RNAs by using the TruSeq RNA sample preparation kit (Illumina, San Diego, CA), and the respective cDNAs were synthesized according to the manufacturer's instructions. The cDNAs fused with an adaptor on both ends were PCR-amplified (15 cycles) and used for sequencing analysis (Illumina HiSeq2000). The obtained

sequence reads (60927373 reads for WT uncut, 59284653 reads for amputated WT at 6 hpa, 58507894 reads for amputated *clo* mutant at 6 hpa) were aligned to the zebrafish reference sequence by using Bowtie software (version 0.12.7; RRID:SCR_005476) (*Langmead et al., 2009*). The normalized expression level of the respective genes, RPKM (reads per kilobase of exon model per million mapped reads), was calculated using ERANGE software (version 3.2; RRID:SCR_005240) (*Mortazavi et al., 2008*).

MO injection

MOs (Gene Tools, Philomath, OR) were dissolved in Danieau solution. Fertilized zebrafish eggs were dechorionated by incubating them with 2% pronase (Roche) and then microinjected at the 1–2-cell stages. The following MOs were used in this study:

irf8 MO: 5′-AATGTTTCGCTTACTTTGAAAATGG-3′ (*Hall et al., 2014*)

csf3r MO1: 5′-ATTCAAGCACATACTCAC-TTCCATT-3′ (*Hall et al., 2014*)

csf3r MO2: 5′- GAACTGGCGGATCTGTAAAGACAAA -3′ (*Halloum et al., 2016*)

spi1b MO: 5′-GATATACTGATACTCCATTGGTGGT-3′ (*Rhodes et al., 2005*)

il1b MO1: 5′-CCCACAAACTGCA-AAATATCAGCTT-3′ (*Nguyen-Chi et al., 2014*)

il1b MO2: 5′- AAACGTAAAATAACTCACCATTGCA -3′ (*Yan et al., 2014*)

std MO: 5′-CCTCTTACCTCAGTTACAATTTATA-3′

The *csf3r* MO2 (0.25 mM) and the rest of MOs (1 mM) were injected at approximately 0.5 nl per egg. Under these conditions, no apparent side effect was observed in our hands. Injected embryos were incubated in 0.3× Niu-Twitty solution.

RT-PCR analysis

Total RNAs were extracted from larval tail tissues (200 for each) posterior to the yolk extension by using TRIzol and further purified using the RNeasy kit (Qiagen, Venlo, Netherlands). Among the purified total RNAs, aliquots that corresponded to 90 larval tails were used for cDNA synthesis. The cDNAs were synthesized by using the Thermoscript RT-PCR kit (Thermo Fisher Scientific) with

random hexamers as the primer. The synthesized cDNAs were diluted to 0.1 μg/μl and stored at −30°C. PCR was performed according to a standard procedure by using Paq5000 DNA polymerase (Agilent Technologies, Santa Clara, CA), and the products were analyzed using 2% agarose gels. The following primers were used for PCR:

il1b Fw: 5′- GCAGAGGAACTTAACCAGCT -3′

il1b Rv: 5′- TGCCGGTCTCCTTCCTGA -3′

actb1 Fw: 5′- ATGGATGAGGAAATCGCTGCCCTGGTCGTTGACAA -3′

actb1 Rv: 5′- AGAGAGAGCACAGCCTGGATGGCCACATACATGGC -3′

Whole-mount ISH analysis

Whole-mount ISH analysis was performed as described previously (*Hasegawa et al., 2015*), except that 5% polyvinyl alcohol was included in the buffer during the color reaction. After detection of the ISH signal, the samples were fixed with 4% paraformaldehyde (PFA) in phosphate-buffered saline (PBS) for color preservation, equilibrated with 80% glycerol, and then mounted on glass slides and photographed. The antisense *junba*, *junbb*, *fn1b*, *apoeb, mpx* and *lcp1* (*l-plastin*) probes used here were described previously (*Yoshinari et al., 2009; Hall et al., 2012*). The *egfp* probe was synthesized from the construct pCS2-egfp, which contained the full-length *egfp* coding sequence. The *il1b* probe was directly synthesized from the *il1b* PCR product by using the T7 promoter (underlined in the primer sequence) (*Thisse and Thisse, 2008*).

il1b probe Fw: 5′-ATGGCATGCGGGCAATATGA-3′

il1b probe Rv: 5′-TAATACGACTCACTATAGGGCTAGATGCGCACTTTATCCT-3′

For preparing tissue sections, samples were incubated in 20% sucrose in PBS for overnight at 4°C, embedded in Tissue-Tek compound (Miles) and 16-μm sections were obtained using a cryostat.

LPS injection

S. typhosa LPS (Sigma–Aldrich, St. Louis, MO) was dissolved in water at 10 mg/ml and stored in aliquots at −30°C. A solution containing LPS (5 mg/ml) and phenol red (0.5%) was injected at 0.5 nl

per larva into the pericardial cavity of anesthetized larvae at 2 dpf.

Generation of Tg lines

The construct for generating Tg(*hsp70l:mCherry-2a-il1b*) was prepared by replacing the *creERt2* sequence of pT2(*hsp70l:mCherry-2a-creERt2*) (*Yoshinari et al., 2012*) with the *il1b* cassette. The *il1b* cassette was prepared by PCR-amplifying the *il1b* sequence a.a. 125–273. The signal sequence of the human IL-1β receptor antagonist (*Wingren et al., 1996*) and the HA tag were fused at the N-terminus and C-terminus, respectively (underlined in the primer sequences).

Fw *il1b* primer:

5′-GCTAGCATGGAAATCTGCAGAGGCCTCCGCAGTCACCTAATCACTCTCCTCCTCTTCCT GTTCCATTCAGAGACGATCTGCAAAAACGTCTTGCAATGCACGATTTGCG-3′

Rv *il1b* primer:

5′-AGATCTCTAAGCGTAGTCTGGGACGTCGTATGGGTAGATGCGCACTTTATCCTGCAGCT CGAAG-3′

The construct was injected into fertilized eggs. To identify germ-line transmission, the F0 fish were crossed with each other or with WT, and the embryos produced were screened for mCherry fluorescence after heat shock.

To generate Tg(*il1b:egfp*), the *iTol2* cassette was first introduced into the BAC clone CH211-147H23 by using BAC recombineering (*Suster et al., 2011*). Next, the *egfp-nitroreductase* cassette (*Grohmann et al., 2009*) was introduced into the site of the initiation codon of *il1b*. Lastly, a mixture of purified BAC DNA (125 ng/μl) and the transposase mRNA (25 ng/μl) was injected into 1-cell-stage zebrafish embryos (1 nl/embryo). The Tg was screened for EGFP expression in the lens, which is driven by the *crystalline alpha* promoter, and further tested for EGFP induction in response to fin fold amputation.

Whole-mount immunohistochemistry

Zebrafish larvae were fixed with 4% PFA in PBS for 2 h at room temperature (RT) or overnight at

4°C, washed thrice with PBS containing 0.1% Triton X-100 (PBTx), dehydrated with methanol, and stored at −30°C. Samples were rehydrated with PBTx and then incubated (overnight, 4°C) with anti-E-cadherin (1:1000; BD Biosciences, Franklin Lakes, NJ; RRID:AB_397580) and anti-EGFP (1:1000; Nacalai Tesque, Kyoto, Japan; RRID:AB_10013361) antibodies in blocking buffer (5% serum and 0.2% bovine serum albumin in PBTx). After extensive washing with PBTx at RT, the samples were incubated (overnight, 4°C) with anti-mouse Alexa Fluor 568 and anti-rat Alexa Fluor 488 antibodies (both 1:1000; Invitrogen). After washing with PBTx, the tail regions were isolated and mounted in 80% glycerol containing 2.5% 1,4-diazabicyclo[2.2.2]octane (Nacalai Tesque) as an anti-fading reagent. Fluorescence images were acquired using a confocal microscope (FV-1000, Olympus, Tokyo, Japan).

Time-lapse analysis of Tg(*il1b:egfp*)

Zebrafish larvae of the BAC Tg(*il1b:egfp*) line at 1 hpa were placed on a 2% agarose-gel stage in egg water and embedded in 0.7% low-melting agarose. Time-lapse images were acquired once every 15 min by using the confocal microscope equipped with a 20× water-immersion objective lens; the acquired images were z-stacks containing 20 optical slices.

TUNEL staining

Larvae were fixed with 4% PFA for 2 h at RT or overnight at 4°C, dehydrated with methanol, and stored at −30°C. Apoptosis was examined using an *in situ* apoptosis detection kit (Roche, Basel, Switzerland). Briefly, samples were rehydrated with PBTx, treated with 10 μg/ml Proteinase K in PBTx (5 min, RT), washed with PBTx, and refixed with 4% PFA in PBS (20 min). The samples were further incubated (15 min, on ice) in a freshly prepared 0.1% sodium citrate buffer containing 0.1% Triton X-100, washed with PBTx, and reacted with the TUNEL reaction mixture at 37°C for 1.5 h. The reaction was terminated by washing with PBTx. The samples were mounted in 80% glycerol and fluorescence images were acquired using confocal microscopy. The TUNEL-positive cells were quantified by counting the number of cells in the area posterior to the notochords.

Chemical treatment

Dex (D-2915; Sigma) was dissolved in dimethyl sulfoxide (DMSO) at 100 mM and stored at −30°C. The Dex solution was diluted to 100 μM with egg water and administered to zebrafish larvae at least 1 h before fin fold amputation.

Sudan Black B staining

Larvae were fixed with 4% PFA for 1 h at RT, rinsed with PBS, and incubated in 0.03% Sudan Black B (Sigma). After extensive washing with 70% ethanol and rehydration with PBS containing 0.1% Tween 20 (PBT), samples were mounted in 80% glycerol.

BrdU staining

Proliferating cells were labeled with 5-bromo-2-deoxyuridine (BrdU, 5 mM) during 0–12 hpa. The labeled larvae were fixed with 4% PFA for 2 h at RT or overnight at 4°C, dehydrated with methanol, and stored at −30°C. Immunochemical detection was performed as described (*Yoshinari et al., 2009*) and BrdU-positive cells were quantified from the acquired confocal images. Similar to the quantification of TUNEL-positive cells, the BrdU-positive cells were quantified by counting the number of cells in the area posterior to the notochords.

Replicates

Most of assessments of phenotypes and expression patterns were replicated in at least two independent experiments with comparable results. Larvae were collected from independent crosses, and experimental processing (injection, heat shock, and/or staining) was carried out on independent occasions. Exceptions to this include data presented in *Figure 1E, Figure 7L*, *Figure 2—figure supplement 1, and Figure 6—figure supplement 1B – D.* In each of these cases, multiple larvae were processed, and the obtained phenotypes were same in all or most of cases. The n is reported within the respective figures.

515

516 **Statistical analysis**

517 Data are presented as means ± SEM. Statistical analyses were performed using Microsoft Excel
518 2013. For normally distributed data, differences were analyzed using Student's *t* tests; $p < 0.05$ was
519 considered statistically significant.

520

521 **Acknowledgements**

522 We thank members of the Kawakami lab. This work was supported by grants from the Koyanagi
523 Foundation and a Grant-in-Aid for Scientific Research (C) to A. Kawakami, by the Marsden Fund
524 grant from the Royal Society of New Zealand to C. J. Hall, and by the NIG-JOINT grant from the
525 National Institute of Genetics to A. Kawakami and K. Kawakami, and by the National BioResource
526 Project from Japan Agency for Medical Research and Development (AMED) to K. Kawakami. T.H.
527 was supported by a fellowship from the Education Academy of Computational Life Science (ACLS)
528 at Tokyo Institute of Technology.

529

530 **Additional information**

531 **Funding**

Funder	Grant reference number	Author
Koyanagi Foundation	15080007	Atsushi Kawakami
Japan Society for the Promotion of Science (JSPS)	Grant-in-Aid for Scientific Research (C)	Atsushi Kawakami
Royal Society of New Zealand	Marsden Fund	Christopher J. Hall
Japan Agency for Medical Research and Development (AMED)	National BioResource Project	Koichi Kawakami

National Institute of Genetics, Japan	NIG-JOINT	Atsushi Kawakami and Koichi Kawakami

The funders had no role in study design, data collection and interpretation, or the decision to submit the work for publication.

532

533

534 **Ethics**

535 This study was performed in strict accordance with the recommendations in the Act on Welfare and
536 Management of Animals in Japan and the Guide for the Care and Use of Laboratory Animals of the
537 National Institutes of Health. All of the animals were handled according to the Animal Research
538 Guidelines at Tokyo Institute of Technology. The protocol was approved by the Committee on the
539 Ethics of Animal Experiments of the Tokyo Institute of Technology. All surgery was performed
540 under tricaine (3-aminobenzoic acid ethyl ester) anesthesia, and every effort was made to minimize
541 suffering.

542

543

References

Bianchi ME. 2007. DAMPs, PAMPs and alarmins: all we need to know about danger. *Journal of Leukocyte Biology* **81**:1-5. doi: 10.1189/jlb.0306164.

Bussmann J, Bakkers J, Schulte-Merker S. 2007. Early endocardial morphogenesis requires Scl/Tal1. *PLoS Genetics* **3**:e140. doi: 10.1371/journal.pgen.0030140.

Dinarello CA. 2009. Immunological and inflammatory functions of the interleukin-1 family. *Annual Review of Immunology* **27**:519-550. doi: 10.1146/annurev.immunol.021908.132612.

Dinarello CA. 2011. Interleukin-1 in the pathogenesis and treatment of inflammatory diseases. *Blood* **117**:3720-3732. doi: 10.1182/blood-2010-07-273417.

Eizirik LD, Mandrup-Poulsen T. 2001. A choice of death – the signal-transduction of immune-mediated beta-cell apoptosis. *Diabetologia* **44**:2115-2133. doi: 10.1007/s001250100021.

Fang Y, Gupta V, Karra R, Holdway JE, Kikuchi K, Poss KD. 2013. Translational profiling of cardiomyocytes identifies an early Jak1/Stat3 injury response required for zebrafish heart regeneration. *Proceedings of the National Academy of Sciences* **110**, 13416-13421. doi: 10.1073/pnas.1309810110.

Gemberling M, Bailey TJ, Hyde DR, Poss KD. 2013. The zebrafish as a model for complex tissue regeneration. *Trends in Genetics* **29**:611-620. doi: 10.1016/j.tig.2013.07.003.

Godwin JW, Pinto AR, Rosenthal NA. 2013. Macrophages are required for adult salamander limb regeneration. *Proceedings of the National Academy of Sciences* **110**:9415-9420. doi: 10.1073/pnas.1300290110.

Goren I, Allmann N, Yogev N, Schürmann C, Linke A, Holdener M, Waisman A, Pfeilschifter J, Frank S. 2009. A transgenic mouse model of inducible macrophage depletion: Effects of diphtheria toxin-driven lysozyme M-specific cell lineage ablation on wound inflammatory, angiogenic, and contractive processes. *The American Journal of Pathology* **175**:132-147. doi: 10.2353/ajpath.2009.081002.

Grohmann M, Paulmann N, Fleischhauer S, Vowinckel J, Priller J, Walther DJ. 2009. A

571 mammalianized synthetic nitroreductase gene for high-level expression. *BMC Cancer* **9**:1-12.
572 doi: 10.1186/1471-2407-9-301.
573 **Hall CJ**, Flores MV, Oehlers SH, Sanderson LE, Lam EY, Crosier KE, Crosier PS. 2012.
574 Infection-responsive expansion of the hematopoietic stem and progenitor cell compartment in
575 zebrafish is dependent upon inducible nitric oxide. *Cell Stem Cell* **10**:198-209. doi:
576 10.1016/j.stem.2012.01.007.
577 **Hall CJ**, Boyle RH, Sun X, Wicker SM, Misa JP, Krissansen GW, Print CG, Crosier KE, Crosier PS.
578 2014. Epidermal cells help coordinate leukocyte migration during inflammation through fatty
579 acid-fuelled matrix metalloproteinase production. *Nature Communications* **5**. doi:
580 10.1038/ncomms4880.
581 **Halloum I**, Carrere-Kremer S, Blaise M, Viljoen A, Bernut A, Le Moigne V, Vilcheze C, Guerardel
582 Y, Lutfalla G, Herrmann JL, Jacobs WR Jr, Kremer L. 2016. Deletion of a dehydratase important
583 for intracellular growth and cording renders rough Mycobacterium abscessus avirulent.
584 *Proceedings of the National Academy of Sciences* **113**: E4228-4237. doi:
585 10.1073/pnas.1605477113.
586 **Hasegawa T**, Nakajima T, Ishida T, Kudo A, Kawakami A. 2015. A diffusible signal derived from
587 hematopoietic cells supports the survival and proliferation of regenerative cells during zebrafish
588 fin fold regeneration. *Developmental Biology* **399**:80-90. doi: 10.1016/j.ydbio.2014.12.015.
589 **Hong S**, Gronert K, Devchand PR, Moussignac RL, Serhan CN. 2003. Novel docosatrienes and
590 17S-resolvins generated from docosahexaenoic acid in murine brain, human blood, and glial cells.
591 Autacoids in anti-inflammation. *The Journal of biological chemistry* **278**: 14677-14687. doi:
592 10.1074/jbc.M300218200.
593 **Ishida T**, Nakajima T, Kudo A, Kawakami A. 2010. Phosphorylation of Junb family proteins by the
594 Jun N-terminal kinase supports tissue regeneration in zebrafish. *Developmental Biology*
595 **340**:468-479. doi: 10.1016/j.ydbio.2010.01.036.
596 **Kanjanamekanant K**, Luckprom P, Pavasant P. 2013. Mechanical stress-induced interleukin-1beta
597 expression through adenosine triphosphate/P2X7 receptor activation in human periodontal

598 ligament cells. *Journal of Periodontal Research* **48**:169-176. doi:
599 10.1111/j.1600-0765.2012.01517.x.
600 **Karra R**, Knecht AK, Kikuchi K, Poss KD. 2015. Myocardial NF-κB activation is essential for
601 zebrafish heart regeneration. *Proceedings of the National Academy of Sciences* **112**, 13255-13260.
602 doi: 10.1073/pnas.1511209112.
603 **Kawakami A**, Fukazawa T, Takeda H. 2004. Early fin primordia of zebrafish larvae regenerate by a
604 similar growth control mechanism with adult regeneration. *Developmental Dynamics*
605 **231**:693-699. doi: 10.1002/dvdy.20181.
606 **Kern JA**, Lamb RJ, Reed JC, Daniele RP, Nowell PC. 1988. Dexamethasone inhibition of
607 interleukin 1 beta production by human monocytes. Posttranscriptional mechanisms. *Journal of*
608 *Clinical Investigation* **81**:237-244. doi: 10.1172/JCI113301.
609 **King MW,** Neff AW, Mescher AL. 2012. The developing Xenopus limb as a model for studies on
610 the balance between inflammation and regeneration. *The Anatomical Record* **295**:1552-1561. doi:
611 10.1002/ar.22443.
612 **Koh TJ**, DiPietro LA. 2011. Inflammation and wound healing: The role of the macrophage. *Expert*
613 *Reviews in Molecular Medicine* **13**:e23-e23. doi: 10.1017/S1462399411001943.
614 **Kolaczkowska E**, Kubes P. 2013. Neutrophil recruitment and function in health and inflammation.
615 *Nature Reviews Immunology* **13**:159-175. doi: 10.1038/nri3399.
616 **Kupper TS**, Ballard DW, Chua AO, McGuire JS, Flood PM, Horowitz MC, Langdon R, Lightfoot L,
617 Gubler U. 1986. Human keratinocytes contain mRNA indistinguishable from monocyte
618 interleukin 1 alpha and beta mRNA. Keratinocyte epidermal cell-derived thymocyte-activating
619 factor is identical to interleukin 1. *The Journal of Experimental Medicine* **164**:2095-2100.
620 **Kyritsis N**, Kizil C, Zocher S, Kroehne V, Kaslin J, Freudenreich D, Iltzsche A, Brand M. 2012.
621 Acute inflammation initiates the regenerative response in the adult zebrafish brain. *Science*
622 **338**:1353-1356. doi: 10.1126/science.1228773.
623 **Langmead B**, Trapnell C, Pop M, Salzberg SL. 2009. Ultrafast and memory-efficient alignment of
624 short DNA sequences to the human genome. *Genome Biology* **10**:R25-R25. doi:

10.1186/gb-2009-10-3-r25.

Li L, Yan B, Shi YQ, Zhang WQ, Wen ZL. 2012. Live imaging reveals differing roles of macrophages and neutrophils during zebrafish tail fin regeneration. *The Journal of Biological Chemistry* **287**:25353-25360. doi: 10.1074/jbc.M112.349126.

Liao Z, Dong J, Wu W, Yang T, Wang T, Guo L, Chen L, Xu D, Wen F. 2012. Resolvin D1 attenuates inflammation in lipopolysaccharide-induced acute lung injury through a process involving the PPARγ/NF-κB pathway. *Respiratory Research* **13**: 110-110. doi: 10.1186/1465-9921-13-110.

Lu YC, Yeh WC, Ohashi PS. 2008. LPS/TLR4 signal transduction pathway. *Cytokine* **42**:145-151. doi: 10.1016/j.cyto.2008.01.006.

Mateus R, Pereira T, Sousa S, de Lima JE. Pascoal S, Saude L, Jacinto A. 2012. In vivo cell and tissue dynamics underlying zebrafish fin fold regeneration. *PloS One* **7**:e51766. doi: 10.1371/journal.pone.0051766.

Mathew LK, Sengupta S, Franzosa JA, Perry J, La Du J, Andreasen EA, Tanguay RL. 2009. Comparative expression profiling reveals an essential role for raldh2 in epimorphic regeneration. *The Journal of Biological Chemistry* **284**:33642-33653. doi: 10.1074/jbc.M109.011668.

Mathew LK, Sengupta S, Kawakami A, Andreasen EA, Lohr CV, Loynes CA, Renshaw SA, Peterson RT, Tanguay RL. 2007. Unraveling tissue regeneration pathways using chemical genetics. *The Journal of Biological Chemistry* **282**:35202-35210. doi: 10.1074/jbc.M706640200

Mortazavi A, Williams BA, McCue K, Schaeffer L, Wold B. (2008). Mapping and quantifying mammalian transcriptomes by RNA-Seq. *Nature Methods* **5**:621-628. doi: 10.1038/nmeth.1226.

Nguyen-Chi M, Phan QT, Gonzalez C, Dubremetz JF, Levraud JP, Lutfalla G. 2014. Transient infection of the zebrafish notochord with E. coli induces chronic inflammation. *Disease Models & Mechanisms* **7**:871-882. doi: 10.1242/dmm.014498.

Ogryzko NV, Hoggett EE, Solaymani-Kohal S, Tazzyman S, Chico TJ, Renshaw SA, Wilson HL. 2014. Zebrafish tissue injury causes upregulation of interleukin-1 and caspase-dependent amplification of the inflammatory response. *Disease Models & Mechanisms* **7,** 259-264. doi:

652 10.1242/dmm.013029.
653 **Okamoto M**, Liu W, Luo Y, Tanaka A, Cai X, Norris DA, Dinarello CA, Fujita M. 2010.
654 Constitutively active inflammasome in human melanoma cells mediating autoinflammation via
655 caspase-1 processing and secretion of interleukin-1beta. *The Journal of Biological Chemistry*
656 **285**:6477-6488. doi: 10.1074/jbc.M109.064907.
657 **Ortega-Gómez A**, Perretti M, Soehnlein O. 2013. Resolution of inflammation: an integrated view.
658 *EMBO Molecular Medicine* **5**:661-674. doi: 10.1002/emmm.201202382.
659 **Petrie TA**, Strand NS, Tsung-Yang C, Rabinowitz JS, Moon RT. 2014. Macrophages modulate adult
660 zebrafish tail fin regeneration. *Development* **141**:2581-2591. doi: 10.1242/dev.098459.
661 **Poss KD**, Keating MT, Nechiporuk A. 2003. Tales of regeneration in zebrafish. *Developmental*
662 *Dynamics* **226**:202-210. doi: 10.1242/dev.098459.
663 **Reischauer S**, Stone OA, Villasenor A, Chi N, Jin SW, Martin M, Lee MT, Fukuda N, Marass M,
664 Witty A. Fiddes I, Kuo T, Chung WS, Salek S, Lerrigo R, Alsiö J, Luo S, Tworus D, Augustine
665 SM, Mucenieks S, Nystedt B, Giraldez AJ, Schroth GP, Andersson O, Stainier DY. 2016. Cloche
666 is a bHLH-PAS transcription factor that drives haemato-vascular specification. *Nature*
667 **535**:294-298. doi: 10.1038/nature18614.
668 **Rhodes J**, Hagen A, Hsu K, Deng M, Liu TX, Look AT, Kanki JP. 2005. Interplay of pu.1 and gata1
669 determines myelo-erythroid progenitor cell fate in zebrafish. *Developmental Cell* **8**: 97-108. doi:
670 10.1016/j.devcel.2004.11.014.
671 **Rock KL**, Kono H. 2008. The inflammatory response to cell death. *Annual Review of Pathology*
672 **3**:99-126. doi: 10.1146/annurev.pathmechdis.3.121806.151456.
673 **Rojas-Munoz A**, Rajadhyksha S, Gilmour D, van Bebber F, Antos C, Rodriguez Esteban C,
674 Nusslein-Volhard C, Izpisua Belmonte JC. 2009. ErbB2 and ErbB3 regulate amputation-induced
675 proliferation and migration during vertebrate regeneration. *Developmental Biology* **327**:177-190.
676 doi: 10.1016/j.ydbio.2008.12.012.
677 **Saraiva M**, O'Garra A. 2010. The regulation of IL-10 production by immune cells. *Nature Reviews*
678 *Immunology* **10**, 170-181. doi:10.1038/nri2711.

679 **Sedger LM**, McDermott MF. 2014. TNF and TNF-receptors: From mediators of cell death and
680 inflammation to therapeutic giants – past, present and future. *Cytokine & Growth Factor Reviews*
681 **25**:453-472. doi: 10.1016/j.cytogfr.2014.07.016.
682 **Serhan CN**, Chiang N, Van Dyke TE. 2008. Resolving inflammation: dual anti-inflammatory and
683 pro-resolution lipid mediators. *Nature Reviews Immunology* **8**:349-61. doi: 10.1038/nri2294.
684 **Shibata E**, Yokota Y, Horita N, Kudo A, Abe G, Kawakami K, Kawakami A. 2016. Fgf signalling
685 controls diverse aspects of fin regeneration. *Development* **143**:2920-9. doi: 10.1242/dev.140699.
686 **Stainier DY**, Weinstein BM, Detrich HW 3rd, Zon LI, Fishman MC. 1995. Cloche, an early acting
687 zebrafish gene, is required by both the endothelial and hematopoietic lineages. *Development*
688 **121**:3141-3150.
689 **Suster ML**, Abe G, Schouw A, Kawakami K. 2011. Transposon-mediated BAC transgenesis in
690 zebrafish. *Nature Protocols* **6**:1998-2021. doi: 10.1038/nprot.2011.416.
691 **Thisse C**, Thisse B. 2008. High-resolution in situ hybridization to whole-mount zebrafish embryos.
692 *Nature Protocols* **3**:59-69. doi: 10.1038/nprot.2007.514.
693 **Tu S**, Bhagat G, Cui G, Takaishi S, Kurt-Jones EA, Rickman B, Betz KS, Penz-Oesterreicher M,
694 Bjorkdahl O, Fox JG. Wang TC. 2008. Overexpression of interleukin-1beta induces gastric
695 inflammation and cancer and mobilizes myeloid-derived suppressor cells in mice. *Cancer Cell*
696 **14**:408-419. doi: 10.1016/j.ccr.2008.10.011.
697 **Vojtech LN**, Scharping N, Woodson JC, Hansen JD. 2012. Roles of inflammatory caspases during
698 processing of zebrafish interleukin-1beta in Francisella noatunensis infection. *Infection and*
699 *Immunity* **80**:2878-2885. doi: 10.1128/IAI.00543-12.
700 **Wallach D**, Kang TB, Kovalenko A. 2014. Concepts of tissue injury and cell death in inflammation:
701 a historical perspective. *Nature Reviews Immunology* **14**:51-59. doi: 10.1038/nri3561.
702 **Wang Q**, Zhang H, Zhao B, Fei H. 2009. IL-1beta caused pancreatic beta-cells apoptosis is mediated
703 in part by endoplasmic reticulum stress via the induction of endoplasmic reticulum Ca2+ release
704 through the c-Jun N-terminal kinase pathway. *Molecular and Cellular Biochemistry* **324**:183-190.
705 doi: 10.1007/s11010-008-9997-9.

Wehner D, Weidinger G. 2015. Signaling networks organizing regenerative growth of the zebrafish fin. *Trends in Genetics* **31**:336-343. doi: 10.1016/j.tig.2015.03.012.

Whitehead GG, Makino S, Lien CL, Keating MT. 2005. fgf20 is essential for initiating zebrafish fin regeneration. *Science* **310**:1957-1960. doi: 10.1126/science.1117637.

Wingren AG, Björkdahl O, Labuda T, Björk L, Andersson U, Gullberg U, Hedlund G, Sjögren HO, Kalland T, Widegren B, Dohlsten M. 1996. Fusion of a signal sequence to the interleukin-1 beta gene directs the protein from cytoplasmic accumulation to extracellular release. *Cellular Immunology* **169**:226-237. doi: 10.1006/cimm.1996.0113.

Yan B, Han P, Pan L, Lu W, Xiong J, Zhang M, Zhang W, Li L, Wen Z. 2014. IL-1beta and reactive oxygen species differentially regulate neutrophil directional migration and Basal random motility in a zebrafish injury-induced inflammation model. *Journal of immunology* **192**: 5998-6008. doi: 10.4049/jimmunol.1301645.

Yoo SK, Freisinger CM, LeBert DC, Huttenlocher A. 2012. Early redox, Src family kinase, and calcium signaling integrate wound responses and tissue regeneration in zebrafish. *The Journal of Cell Biology* **199**:225-234. doi: 10.1083/jcb.201203154.

Yoshinari N, Kawakami A. 2011. Mature and juvenile tissue models of regeneration in small fish species. *The Biological Bulletin* **221**:62-78. doi: 10.1086/BBLv221n1p62.

Yoshinari N, Ishida T, Kudo A, Kawakami A. 2009. Gene expression and functional analysis of zebrafish larval fin fold regeneration. *Developmental Biology* **325**:71-81. doi: 10.1016/j.ydbio.2008.09.028.

Yu H, Pardoll D, Jove R. 2009. STATs in cancer inflammation and immunity: a leading role for STAT3. *Nature Reviews Cancer* **9**, 798-809. doi:10.1038/nrc2734.

730 **FIGURE LEGENDS**

731 **Figure 1. Prolonged activation of *il1b* expression in the *clo* mutant after fin fold amputation.**
732 (**A**) Transcriptome analysis of posterior fin fold tissues from uncut WT, amputated WT, and
733 amputated *clo* mutant at 6 hpa. The ordinate, final RPKM, indicates the reads per kilobase of exon
734 model per million mapped reads. The expression of regeneration-induced genes such as *fn1b*, *junba*,
735 *junbb*, *mmp9*, and *fgf20a* was upregulated in the *clo* mutant. Notably, the expression of
736 inflammation-related genes such as *il1b*, *tnf1b*, and *ptgs2a* was highly upregulated in the amputated
737 *clo* mutant. (**B**) RT-PCR analysis of *il1b* expression in WT and *clo* larvae at 3, 6 and 12 hpa. *actb1*:
738 *actinb1*. (**C**) ISH analysis of *il1b* expression at corresponding stages of regeneration in WT and *clo*.
739 Arrowheads indicate myeloid-like cells expressing *il1b*. Scale bars, 25 μm. (**D**) Quantification of
740 *il1b* expression. The level of *il1b* expression was divided into 4 groups according to the ISH signal;
741 the numbers in the bars indicate the ratios of the respective groups. Data are sum of 3 experiments
742 (total n > 13 for each sample). The data suggest that *il1b* expression extended into later stages in *clo*
743 than in WT. (**E**) ISH analysis of *il1b* expression after LPS injection. Phenol red: negative control
744 containing only phenol red; hpi: hours post injection. Scale bars, 200 μm.

745
746
747 **Figure 2**. Spatiotemporal expression of *il1b* during fin fold regeneration. (**A**) Tissue cryosection of
748 an amputated *clo* fin fold in which *il1b* expression was detected using ISH analysis. Arrowheads
749 indicate the epidermal cells expressing *il1b*. Scale bar, 10 μm. (**B**) Live imaging of *il1b* expression in
750 the Tg(*il1b*:*egfp*) line in WT and *clo* mutant at corresponding stages of regeneration. As in the case
751 *il1b* expression observed in ISH analysis (*Figure 1C*), EGFP fluorescence of the Tg(*il1b*:*EGFP*) was
752 strongly upregulated in the *clo* mutant. The EGFP fluorescence in WT decreased more slowly than
753 the *il1b* mRNA signal did due to the comparatively longer half-life of the protein EGFP. Scale bars,
754 100 μm. (**C**) Immunofluorescence detection of EGFP and E-cadherin in Tg(*il1b*:*EGFP*) at 3 and 12
755 hpa. Confocal longitudinal and transverse optical sections are shown at the top and right side,
756 respectively. Vertical and horizontal red and green lines indicate the approximate sites of the optical
757 sections. Scale bars, 50 μm.

Figure 3. *il1b* knockdown or Dex treatment rescued the *clo* apoptosis.

(**A**) Simultaneous detection of apoptosis by the TdT-mediated dUTP nick end labeling (TUNEL) and the *il1b*-expressing cell at 12 hpa in the *clo* mutant carrying the transgene *il1b*:*egfp*. Most of the TUNEL-positive cells were detected in close association with the *il1b*-expressing epithelial cells. Vertical and horizontal lines indicate the approximate sites of the optical sections. Scale bar, 100 μm. (**B**) RT-PCR analysis of *il1b* and *actinb1* expression in zebrafish larvae injected with the *il1b* MO. The *il1b* MO was targeted to the splice donor site. Arrowhead indicates the aberrant transcript. (**C**) TUNEL analysis in amputated WT or *clo* larvae (12 hpa) after *il1b* knockdown. Injection of the *il1b* MO substantially reduced the apoptosis of regenerative cells in the *clo* mutant, whereas the apoptosis was unaffected by std MO. Scale bars, 50 μm. (**D**) Quantification of TUNEL staining in the areas bracketed in (C). (**E**) ISH analysis of *il1b* expression at 3 hpa in larvae treated with Dex. DMSO: dimethyl sulfoxide, used as the vehicle. Dex treatment abolished *il1b* expression. Scale bar, 50 μm. (**F**) TUNEL staining in the amputated fin fold at 12 hpa in Dex-treated WT and *clo* larvae. Scale bars, 50 μm. (**G**) Quantification of TUNEL staining in the areas bracketed in (F). In (D) and (G), data are presented as means ± SEM. Student's *t* test, **p < 0.01; ***p < 0.001; N.S., not significant (p = 0.172).

Figure 4. Macrophages are responsible for the survival of regenerative cells.

(**A**) ISH analysis of the *lcp1* expression, a macrophage marker, during fin fold regeneration in WT. Scale bar, 50 μm. (B) ISH analysis of the *mpx* expression, a neutrophil marker, during fin fold regeneration in WT. Scale bar, 50 μm. (**C**) TUNEL analysis in the amputated fin fold at 12 hpa after injection of *spi1b*, *csf3r*, and *irf8* MOs. The injection of *spi1b* MO and *irf8* MO markedly increased the apoptosis of regenerative cells. Scale bar, 100 μm. (**D**) Quantification of TUNEL-positive cells in the areas bracketed in (A). In (B), data are presented as means ± SEM. Student's *t* test, ***p < 0.001; N.S., not significant (p = 0.981).

Figure 5. Prolonged *il1b* expression and apoptosis are induced by macrophage loss during fin fold regeneration.

(**A**) ISH analysis of *il1b* expression in *spi1b*, *csf3r*, and *irf8* morphants. The *spi1b* and *irf8* morphants displayed prolonged *il1b* expression at 6 hpa. Scale bar, 50 μm. (**B**) Quantification of *il1b* expression detected using ISH analysis in (A). The level of *il1b* expression was evaluated as in *Figure 1D*. Data are the sum of 2 experiments (total n > 16 for each MO). (**C**) TUNEL analysis of the amputated fin fold at 12 hpa after *il1b* knockdown or Dex treatment in larvae in which macrophages were depleted using the *spi1b* or *irf8* MO. Scale bar, 100 μm. Apoptosis caused by *spi1b* and *irf8* MOs was rescued by *il1b* MO administration or Dex treatment. (**D**) Quantification of TUNEL staining in the *spi1b* morphants (C; bracketed areas). (**E**) Quantification of TUNEL staining in the *irf8* morphants in (C). In (D) and (E), data are presented as means ± SEM. Student's *t* test, ***$p < 0.001$.

Figure 6. *il1b* overexpression induces aberrant apoptosis.

(**A**) A schematic diagram of the construct used; in this construct, the zebrafish *heat shock protein 70l* promoter drives the expression of *mCherry* and *il1b* harboring a signal sequence. (**B**) mCherry fluorescence in Tg(*hsp70l:il1b*) at 4 hrs after heat shock. WT, sibling WT. Scale bar, 250 μm. (**C**) TUNEL analysis in the amputated fin fold of Tg(*hsp70l:il1b*) at 2 dpa. The diagram depicts the experimental procedure. HS, heat shock. Scale bar, 100 μm. (**D**) Quantification of TUNEL staining in (C). (**E**) Fin fold regeneration in Tg(*hsp70l:il1b*) and sibling WT larvae. Dotted lines indicate amputation planes and fin fold outlines. Scale bar, 100 μm. (**F**) Quantification of the length of the regenerate (length posterior to the amputation plane; shown in (E)). In (D) and (F), data are presented as means ± SEM. Student's *t* test, ***$p < 0.001$.

Figure 7. Il1b-mediated inflammation is required for proper regeneration.

(**A**) Fin fold regeneration in WT larvae treated with Dex. Regeneration was retarded following treatment with Dex but not vehicle DMSO (arrowheads). Scale bar, 100 μm. (**B**) Quantification for (A) (posterior to the notochord). (**C**) BrdU incorporation in larvae treated with DMSO or Dex. BrdU labeling, 0–24 hpa. Scale bar, 50 μm. (**D**) Quantification for (C) (bracketed areas). BrdU-positive cells were significantly reduced following Dex treatment. (**E**) Detection of *junba* expression by using ISH and *fgf20a* expression by using the *HGn21A* enhancer-trap line (*Shibata et al., 2016*) in DMSO- or Dex-treated larvae. The expression of *junba* and *fgf20a* was also significantly downregulated following Dex treatment. Arrowheads indicate EGFP expression in amputated sites. Scale bars, 50 μm (**F**) Fin fold regeneration in larvae injected with std or *il1b* MO. The knockdown of *il1b* reduced fin fold regeneration. Scale bar, 100 μm. (**G**) Quantification for (F) (posterior to the notochord). (**H**) BrdU incorporation in larvae injected with std or *il1b* MO. BrdU labeling, 0–24 hpa. Scale bar, 50 μm. (**I**) Quantification for (H) (bracketed areas). (**J**) Detection of *junba* expression by using ISH and *fgf20a* expression by using the *HGn21A* line in larvae injected with std or *il1b* MO. The expression of *junba* and *fgf20a* was downregulated following *il1b* knockdown as in the Dex-treated larvae. Arrowheads indicate EGFP expression in amputated sites. Scale bars, 50 μm. (**K**) Schematic of the procedure of *il1b* overexpression in uninjured WT larvae. Heat shock was applied twice before fixation. (**L**) ISH analysis of *fn1b*, *junba*, and *junbb* in WT and Tg(*hsp70l:il1b*). *il1b* overexpression stimulated ectopic expression of regeneration-induced genes in uninjured larvae. Scale bar, 50 μm. In (A) and (F), dotted lines indicate amputation planes and fin fold outlines. In (B), (D), (G), and (I), data are presented as means ± SEM. Student's *t* test, **p < 0.01; ***p < 0.001.

Figure 8. Schematic of the role of Il1b and macrophages during fin fold regeneration.

(**A** and **B**) Tissue injury induces *il1b* expression in epithelial cells. The expressed Il1b acts on the surrounding cells to prime them for regeneration by triggering the expression of regeneration-induced genes such as *fn1b*, *junba*, *junbb*, and *fgf20a*. (**C**) The macrophage-derived factor subsequently attenuate *il1b* expression during normal regeneration. (**D**) In the absence of

macrophages, apoptosis is induced in the primed regenerative cells. Thus, the Il1b function is akin to a double-edged sword in tissue regeneration.

Video 1. Time-lapse imaging of EGFP fluorescence in Tg(*il1b*:*egfp*) from 1 to 11 hpa.
Images were acquired once every 15 min. The epidermal cells in the injury site and the migrating cells, which are considered to be myeloid cells, expressed EGFP.

SOURCE DATA Title/legends:

Figure 1 – source Data 1. *il1b* expression at respective time points after fin fold amputation.

The table shows the numbers of larvae used for evaluating the *il1b* expression levels in WT or *clo* mutant at respective time points after fin fold amputation.

Figure 5 – source Data 1. *il1b* expression in larvae injected with std, *spi1b*, *csf3r*, or *irf8* MOs.

The table shows the numbers of larvae used for evaluating the *il1b* expression levels in larvae that were injected with respective MOs.

SUPPLEMENTARY FILES LEGENDS:

Supplementary File 1. The list of transcripts that are upregulated or downregulated in the amputated fin fold of the *clo* mutant.

The table of upregulated genes shows the list of transcripts whose final RPKMs of the amputated *clo* mutant at 6 hpa are more than 2 times than those of the amputated WT. The table of downregulated genes shows the list of top 100 transcripts whose final RPKMs of the amputated *clo* mutant at 6 hpa are downregulated compared to those of amputated WT. Transcripts with low expression in the *clo* mutant (final RPKM < 4) were excluded. Final RPKM, the reads per kilobase of exon model per million mapped reads. Transcripts that are shown in *Figure 1A* are highlighted.

Figure 2 – figure supplement 1. Reproduction of *il1b* expression in the Tg(*il1b*:*egfp*) line.

(**A**) EGFP expression in Tg(*il1b*:*egfp*) at 2 dpa. Arrowheads, EGFP expression in the pectoral fins and the posterior tip of the notochord. Arrow, EGFP expression in the lens by *crystalline alpha A:egfp* inserted in the Tol2 vector. Scale bar, 300 μm. (**B**) ISH analysis of *egfp* and endogenous *il1b* expression in Tg(*il1b*:*egfp*). The two genes were expressed in the same pattern. Scale bar, 50 μm. (**C**) EGFP fluorescence in Tg(*il1b*:*egfp*) after injection of LPS or control solution containing phenol red. Arrowheads indicate some of the EGFP-positive myeloid cells in LPS-injected larvae at 2 dpf; hpi: hours post injection. Scale bar, 100 μm.

Figure 3 – figure supplement 1. Rescue of the *clo* apoptosis by *il1b* MO2.

(**A**) TUNEL analysis of amputated *clo* larvae that were injected with the *il1b* MO2. The *il1b* MO2 rescued the apoptosis of regenerative cells in the *clo* mutant, whereas the apoptosis was unaffected by std MO. Scale bars, 50 μm. (**B**) Quantification of TUNEL-positive cells in the areas bracketed in (A). Data are presented as means ± SEM. Student's t test, ***$p < 0.001$.

889

890 **Figure 4 – figure supplement 1**. **Efficacy of MO-mediated macrophage and/or neutrophil**

891 **depletion.**

892 (**A**) Sudan Black staining in std, *spi1b*, and *csf3r* morphants. Scale bar, 300 μm. Knockdowns by the

893 *spi1b* and *csf3r* MOs decreased the number of neutrophils. (**B**) Quantification of Sudan Black

894 staining (A; posterior to the yolk extension). Data are presented as means ± SEM. Student's *t* test,

895 ***p < 0.001. (**C**) Analysis of *apoeb* expression in std and *irf8* morphants. The *irf8* MO inhibited the

896 differentiation of glial cells marked by *apoeb*. Scale bar, 100 μm. (**D**) ISH analysis of the *mpx*

897 expression, a neutrophil marker, at 2 hpa in amputated fin fold of the larvae injected with std, *spi1b*

898 or *csf3r* MOs. The *mpx*-positive cells were not detected in the *spi1b* or *csf3r* morphants. Arrowheads

899 indicate representative neutrophils. Scale bar, 25 μm. (**E**) ISH analysis of *lcp1*, a macrophage marker,

900 at 6 hpa in amputated fin fold of the larvae injected with std, *spi1b* or *irf8* MOs. Arrowheads indicate

901 representative macrophages migrated to the injured site. The *lcp1*-positive macrophages are rarely

902 observed in amputated fin fold of the *spi1b* or *irf8* morphants. Scale bar, 25 μm.

903

904

905 **Figure 6 – figure supplement 1. Generation of Tg(*hsp:il1b*).**

906 (**A**) Comparison of zebrafish Il1b and human IL-1β amino acid sequences. Arrows indicate the

907 human IL-1β cleavage site (D116) and the estimated zebrafish Il1b cleavage site (T124). (**B**) ISH

908 analysis of *il1b* expression in Tg(*hsp70l:il1b*) at 6 h after heat shock (HS). HS induced systemic *il1b*

909 expression. Scale bar, 250 μm. (**C**) Absence of mCherry induction by fin fold amputation in the

910 Tg(*hsp70l:il1b*). A stress caused by fin fold amputation did not induce mCherry expression. Scale

911 bar, 100 μm. (**D**) TUNEL analysis of Tg(*hsp70l:il1b*) at 24 hpf after induction of *il1b* overexpression.

912 The diagram depicts the experimental procedure. Scale bar, 500 μm.

913

914

915 **Figure 7 – figure supplement 1. Absence of apoptosis after two HS inductions in the**

Tg(*hsp70l:il1b*).

TUNEL analysis after two HS inductions of *il1b* overexpression (*Figure 6K*). At this stage, apoptosis has not been induced yet. Scale bar, 100 μm.

A

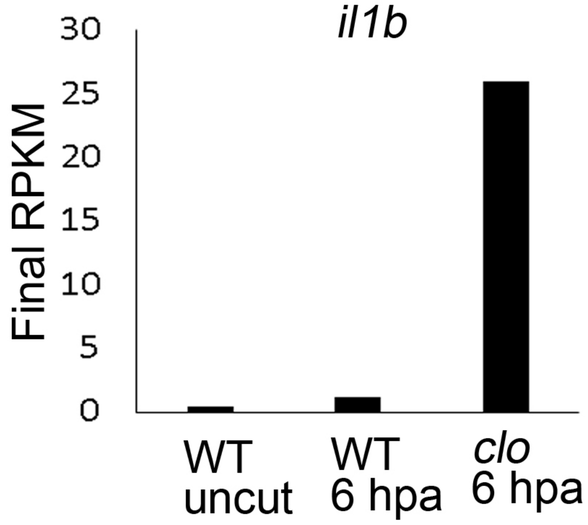
il1b
Final RPKM
30
25
20
15
10
5
0
WT uncut
WT 6 hpa
clo 6 hpa

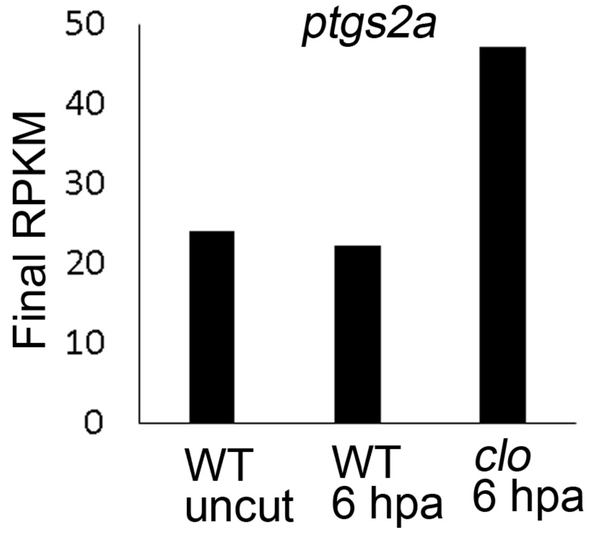
ptgs2a
Final RPKM
50
40
30
20
10
0
WT uncut
WT 6 hpa
clo 6 hpa

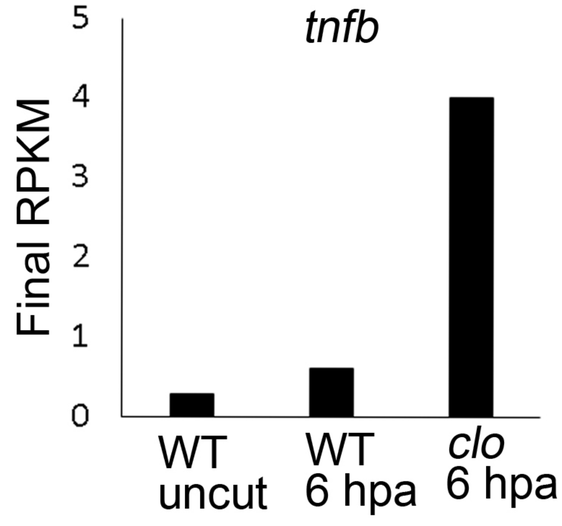
tnfb
Final RPKM
5
4
3
2
1
0
WT uncut
WT 6 hpa
clo 6 hpa

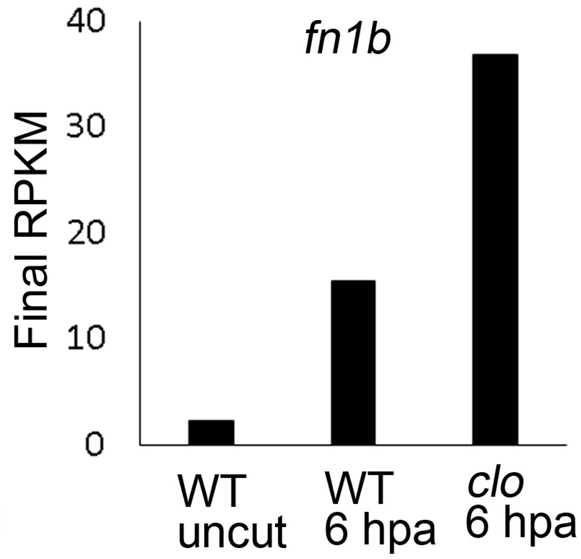
fn1b
Final RPKM
40
30
20
10
0
WT uncut
WT 6 hpa
clo 6 hpa

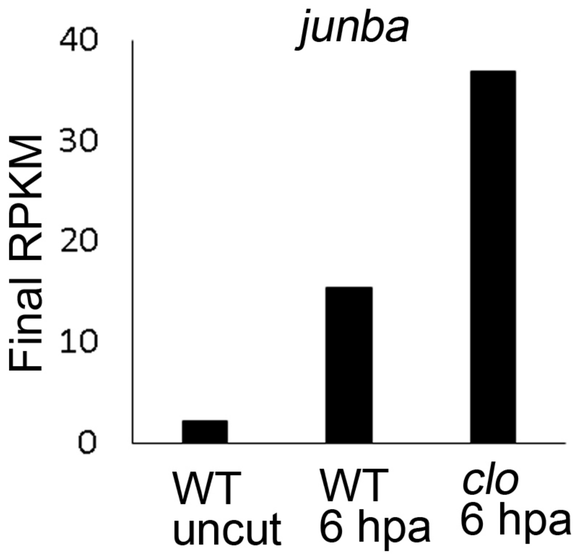
junba
Final RPKM
40
30
20
10
0
WT uncut
WT 6 hpa
clo 6 hpa

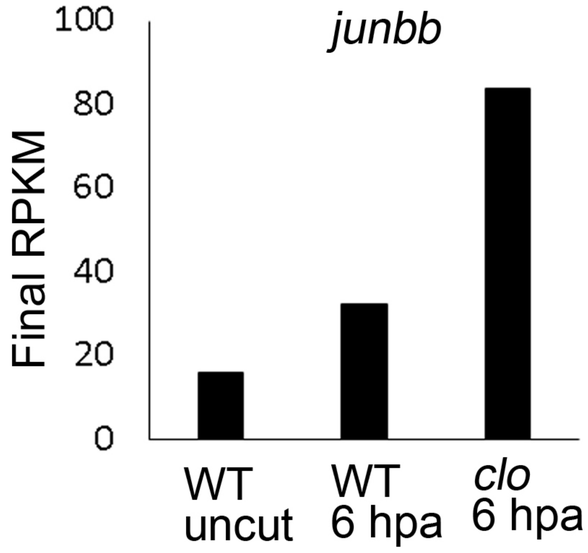
junbb
Final RPKM
100
80
60
40
20
0
WT uncut
WT 6 hpa
clo 6 hpa

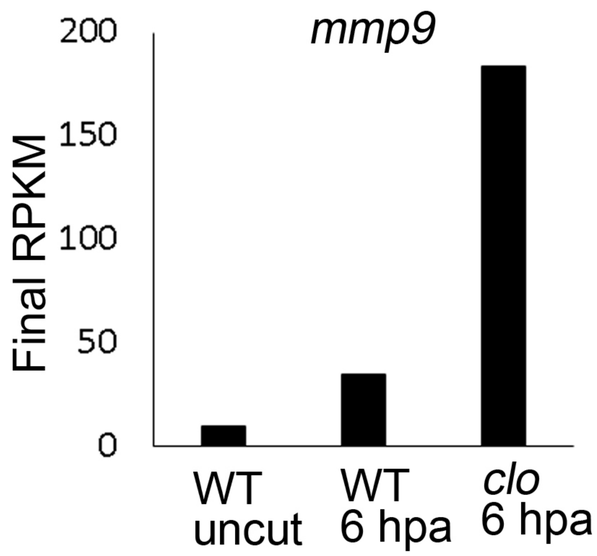
mmp9
Final RPKM
200
150
100
50
0
WT uncut
WT 6 hpa
clo 6 hpa

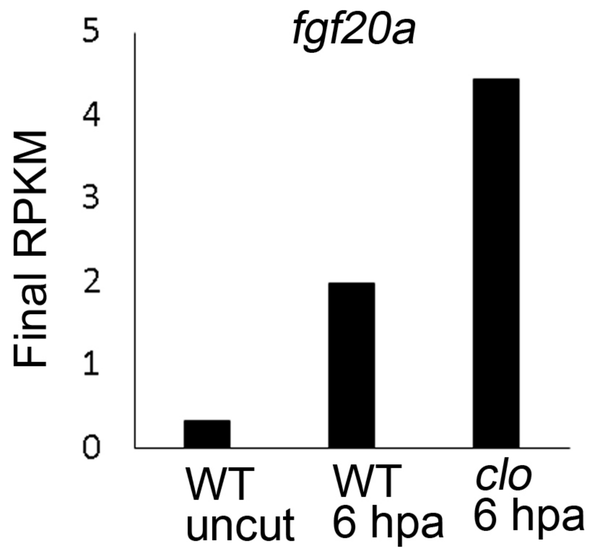
fgf20a
Final RPKM
5
4
3
2
1
0
WT uncut
WT 6 hpa
clo 6 hpa

B

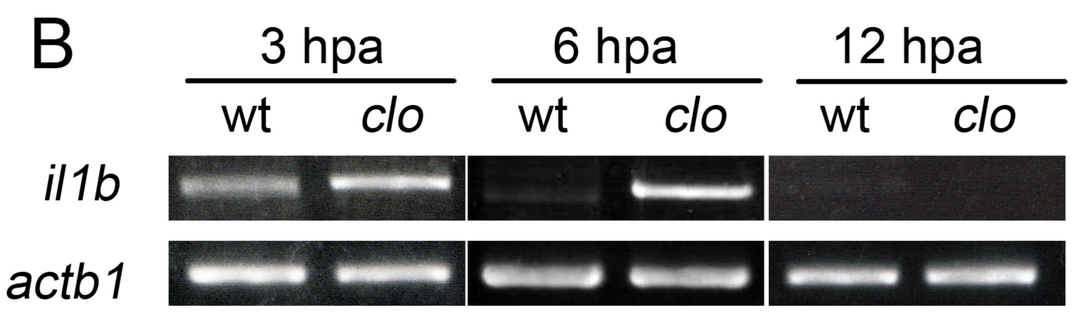
3 hpa
6 hpa
12 hpa
wt
clo
wt
clo
wt
clo
il1b
actb1

C

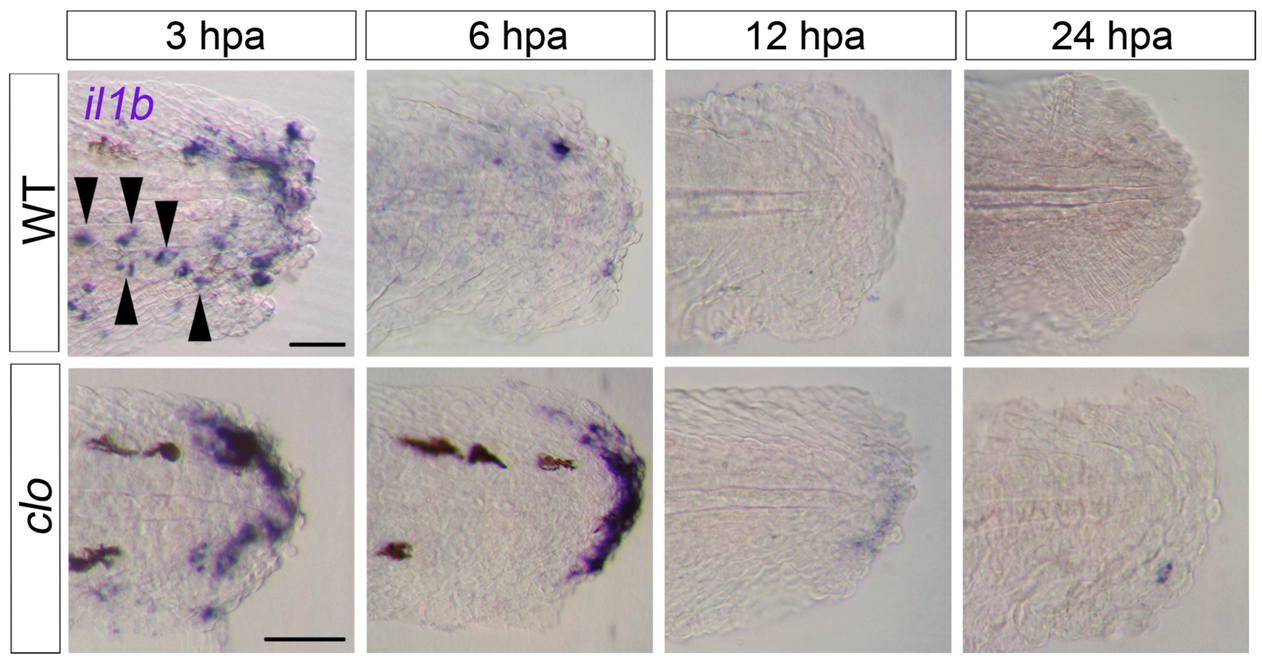
3 hpa
6 hpa
12 hpa
24 hpa
WT
clo
il1b

D

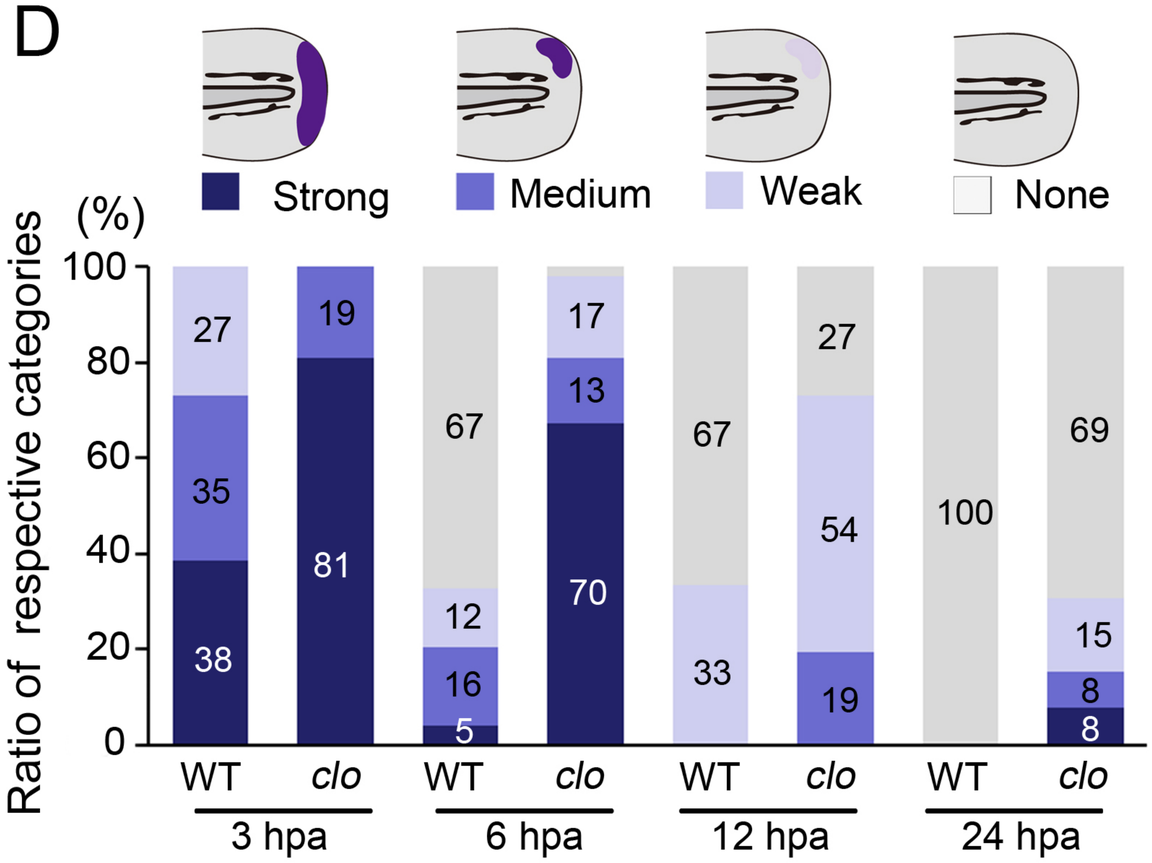
Strong
Medium
Weak
None
(%)
Ratio of respective categories
100
80
60
40
20
0
27
35
38
19
81
67
12
16
5
17
13
70
67
33
27
54
19
100
69
15
8
8
WT
clo
WT
clo
WT
clo
WT
clo
3 hpa
6 hpa
12 hpa
24 hpa

E

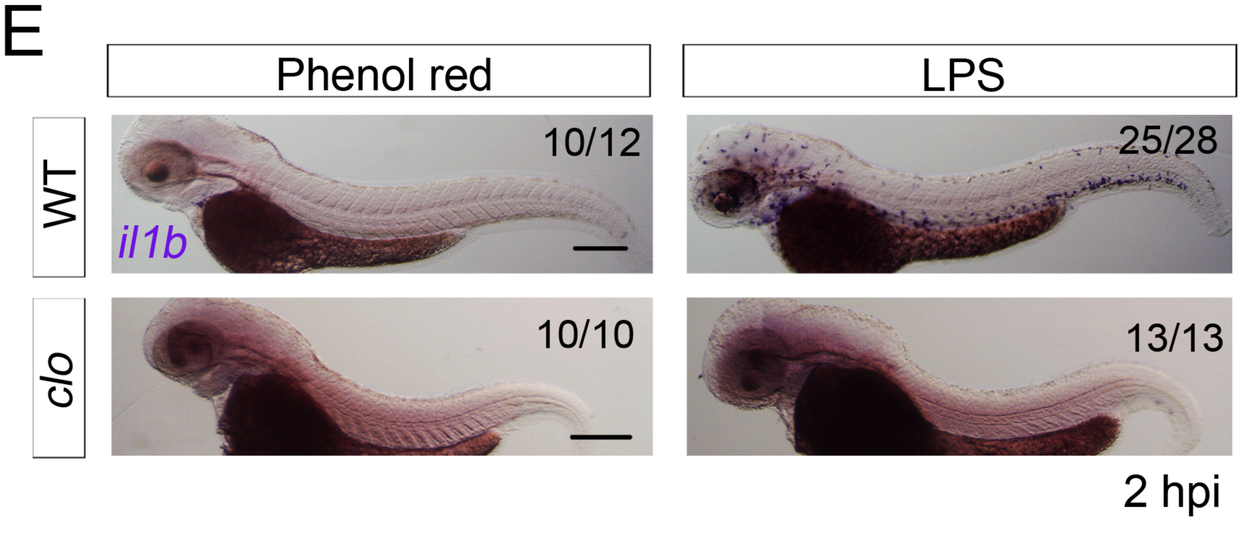
Phenol red
LPS
WT
clo
il1b
10/12
25/28
10/10
13/13
2 hpi

A

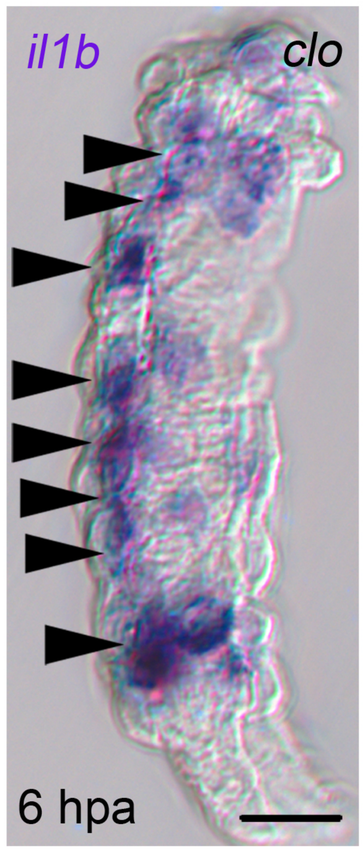
il1b
clo
6 hpa

C

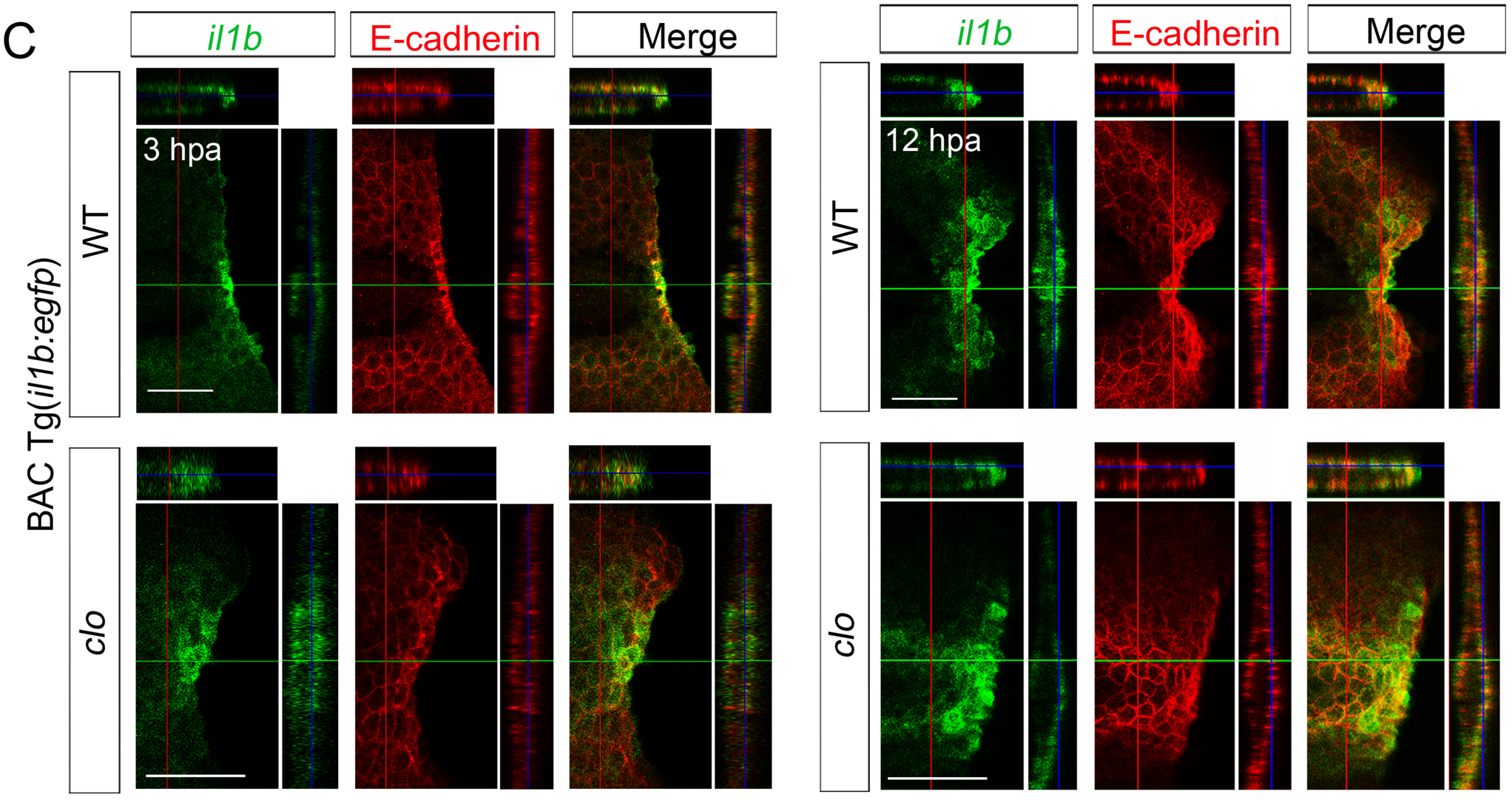
il1b
E-cadherin
Merge
BAC Tg(il1b:egfp)
WT
clo
3 hpa
12 hpa

B

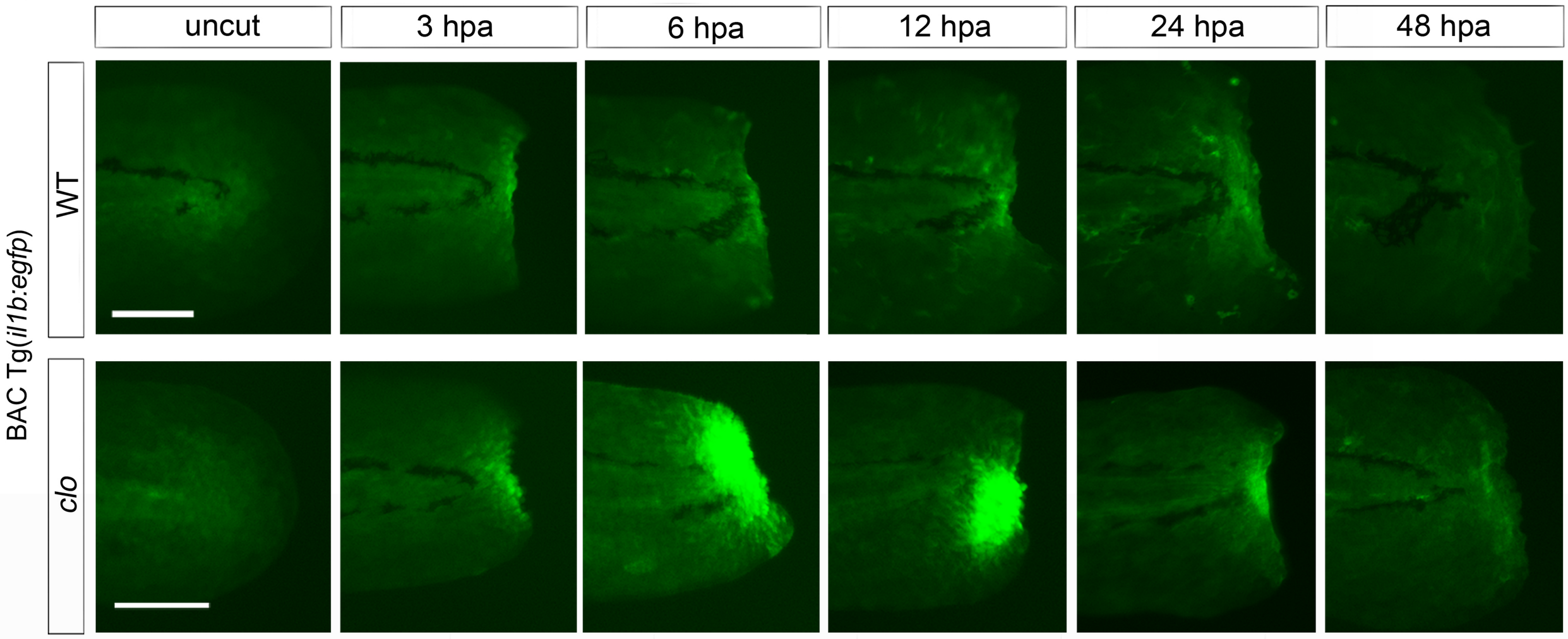
uncut
3 hpa
6 hpa
12 hpa
24 hpa
48 hpa
BAC Tg(il1b:egfp)
WT
clo

A

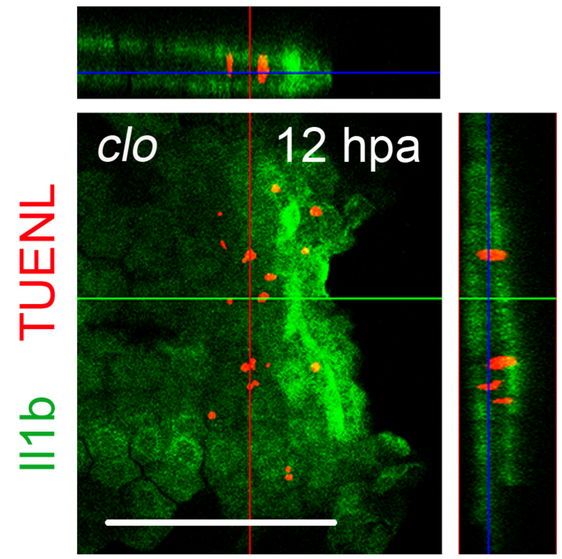
clo
12 hpa
TUENL
Il1b

B

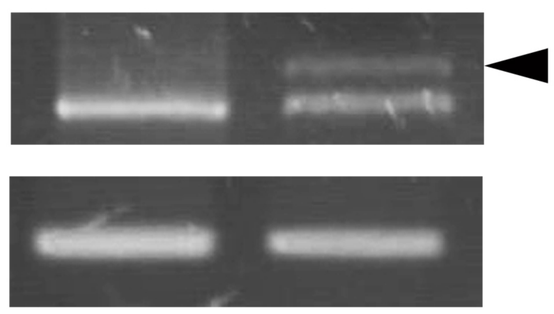
std MO
il1b MO1
il1b
actb1

C

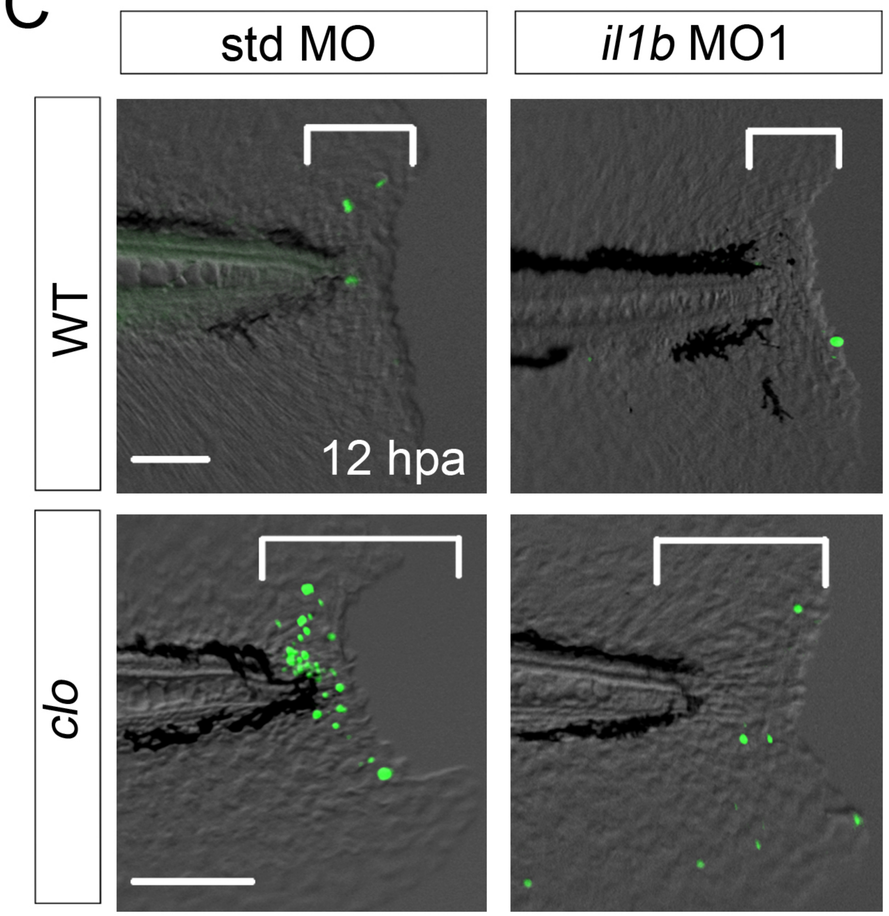
std MO
il1b MO1
WT
clo
12 hpa

D

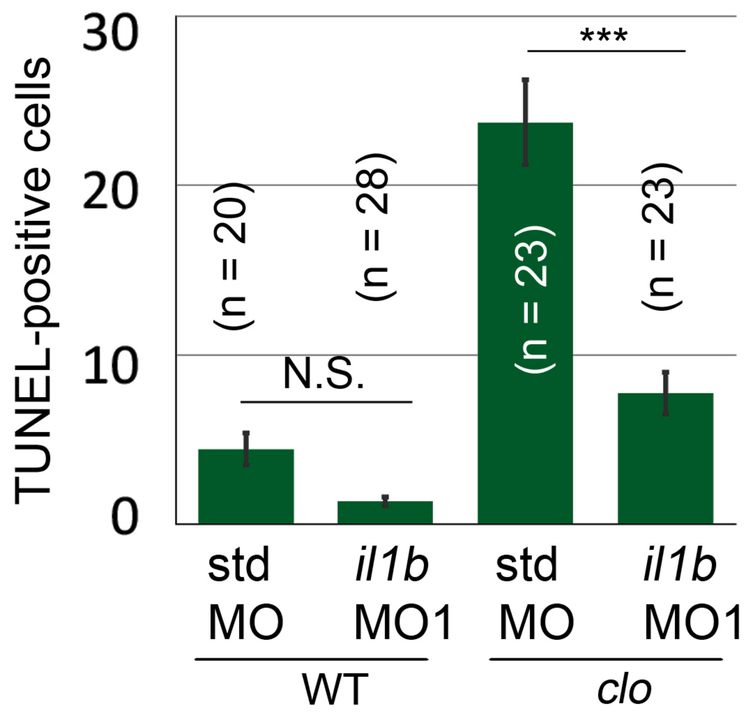
TUNEL-positive cells
30
20
10
0
(n = 20)
(n = 28)
(n = 23)
(n = 23)
N.S.
***
std MO
il1b MO1
std MO
il1b MO1
WT
clo

E

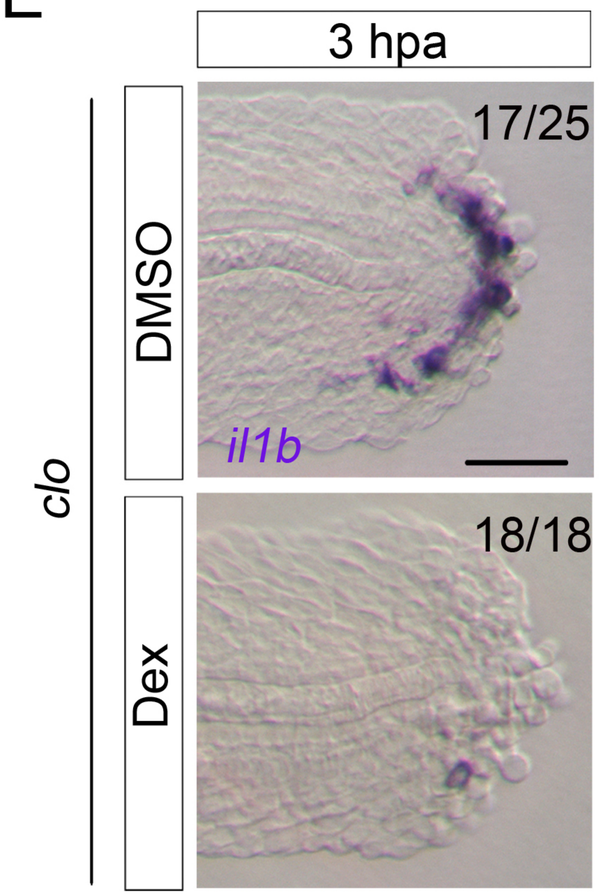
3 hpa
clo
DMSO
Dex
17/25
18/18
il1b

F

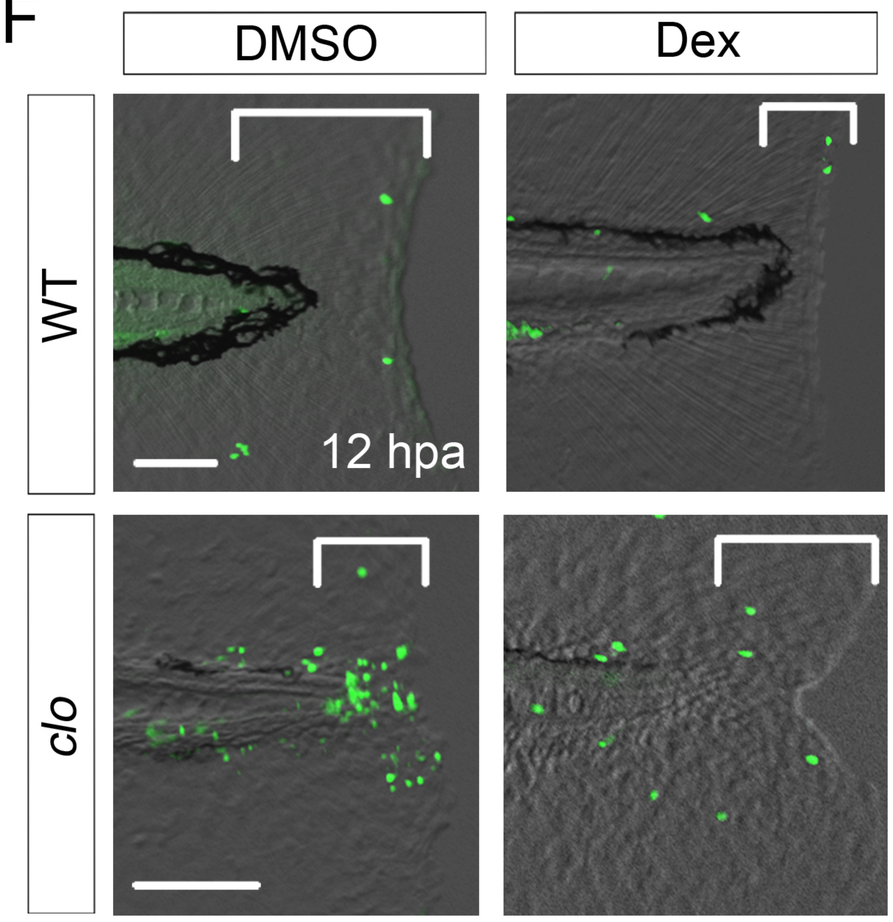
DMSO
Dex
WT
clo
12 hpa

G

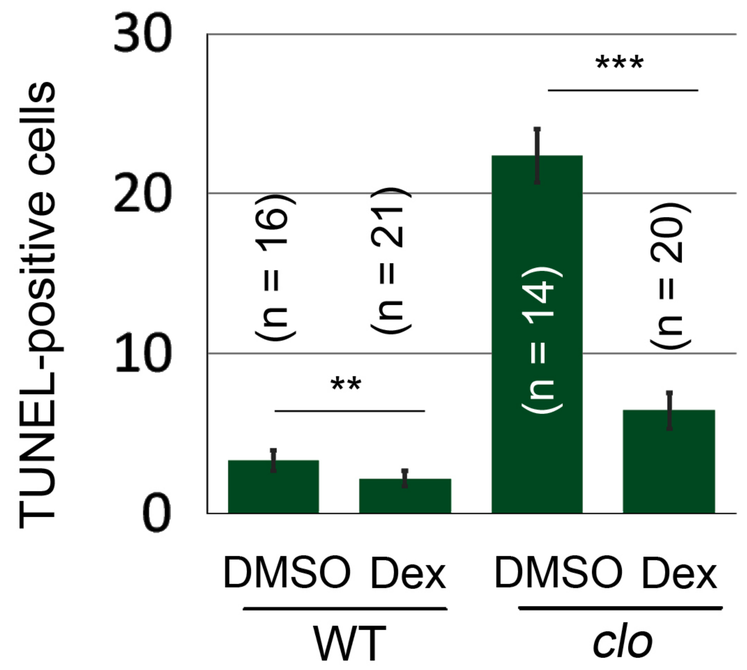
TUNEL-positive cells
30
20
10
0
(n = 16)
(n = 21)
(n = 14)
(n = 20)
**
***
DMSO
Dex
DMSO
Dex
WT
clo

A

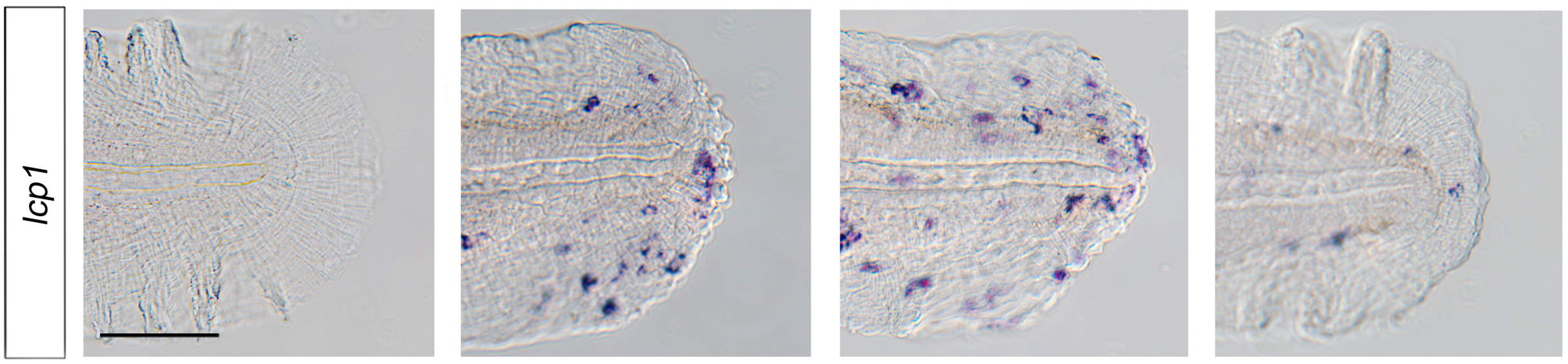
uncut
3 hpa
6 hpa
12 hpa
lcp1

B

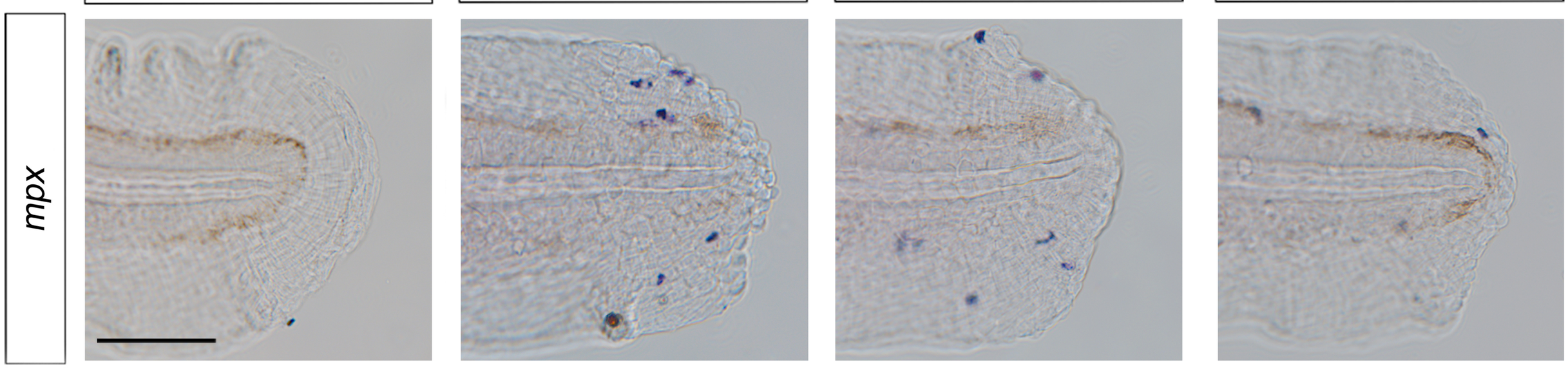
uncut
3 hpa
6 hpa
12 hpa
mpx

C

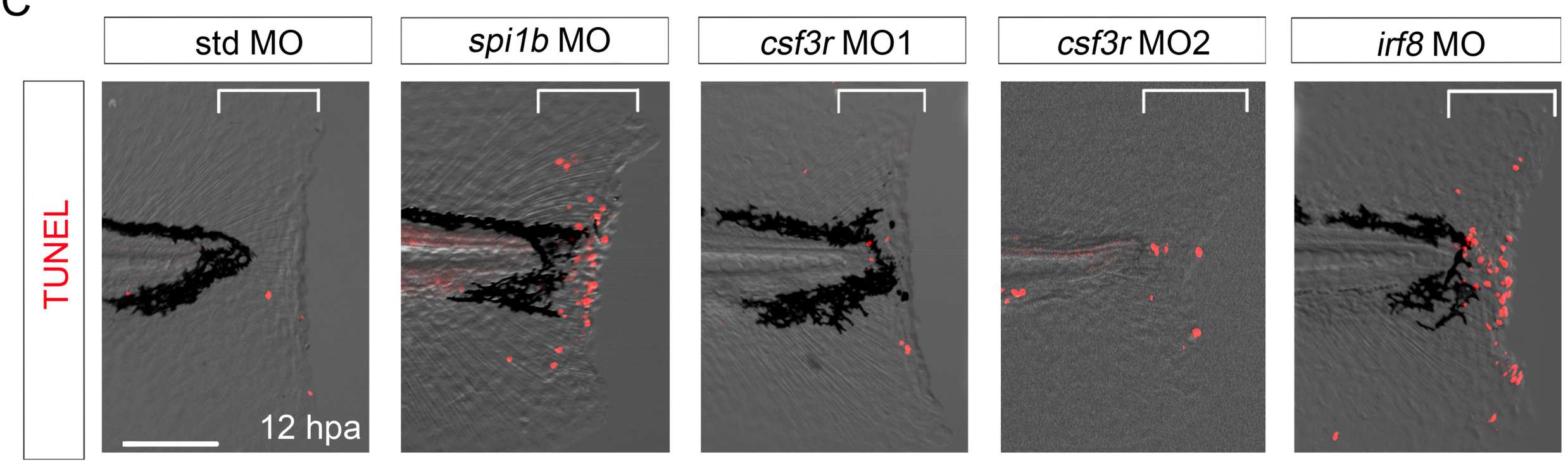
std MO
spi1b MO
csf3r MO1
csf3r MO2
irf8 MO
TUNEL
12 hpa

D

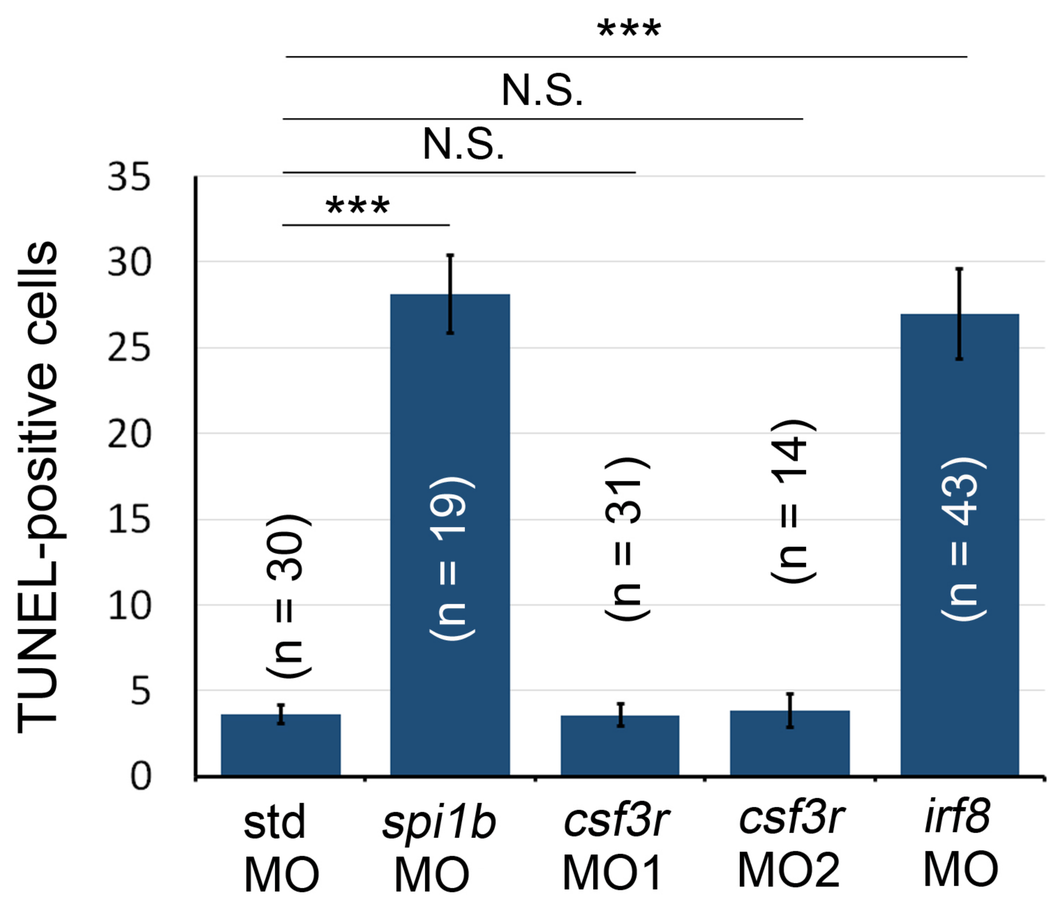
***
N.S.
N.S.
***
TUNEL-positive cells
35
30
25
20
15
10
5
0
(n = 30)
(n = 19)
(n = 31)
(n = 14)
(n = 43)
std MO
spi1b MO
csf3r MO1
csf3r MO2
irf8 MO

A

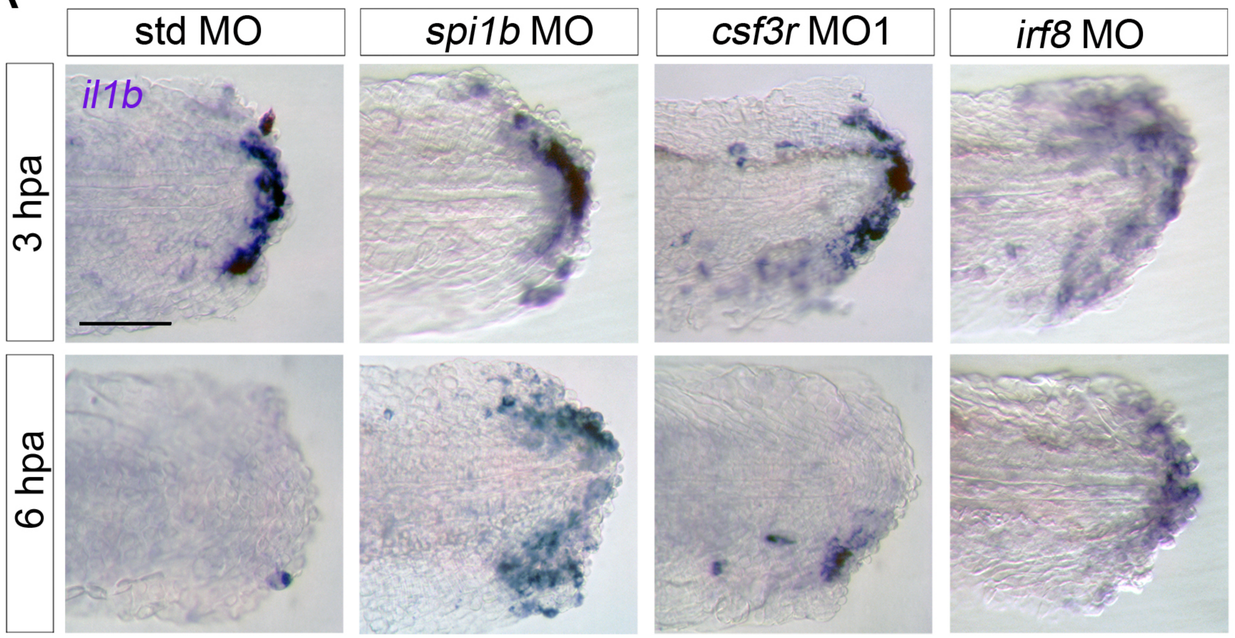
std MO
spi1b MO
csf3r MO1
irf8 MO
3 hpa
6 hpa
il1b

B

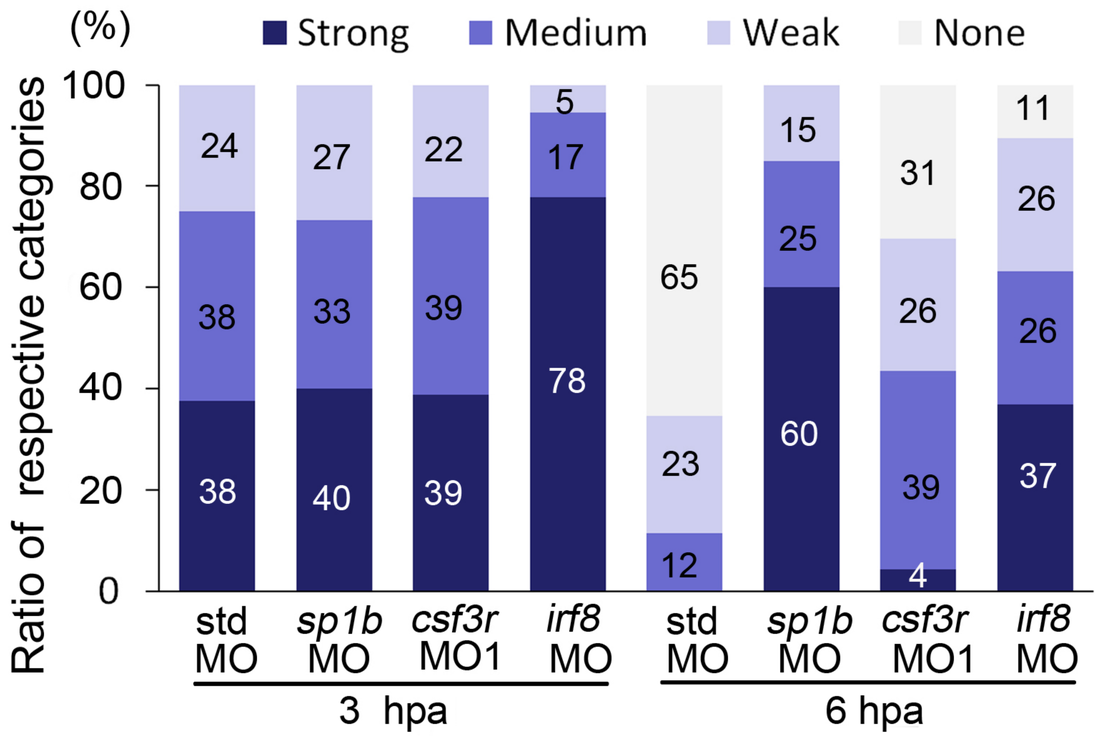
(%)
Strong
Medium
Weak
None
Ratio of respective categories
100
80
60
40
20
0
24
38
38
27
33
40
22
39
39
5
17
78
65
23
12
15
25
60
31
26
39
4
11
26
26
37
std MO
sp1b MO
csf3r MO1
irf8 MO
std MO
sp1b MO
csf3r MO1
irf8 MO
3 hpa
6 hpa

C

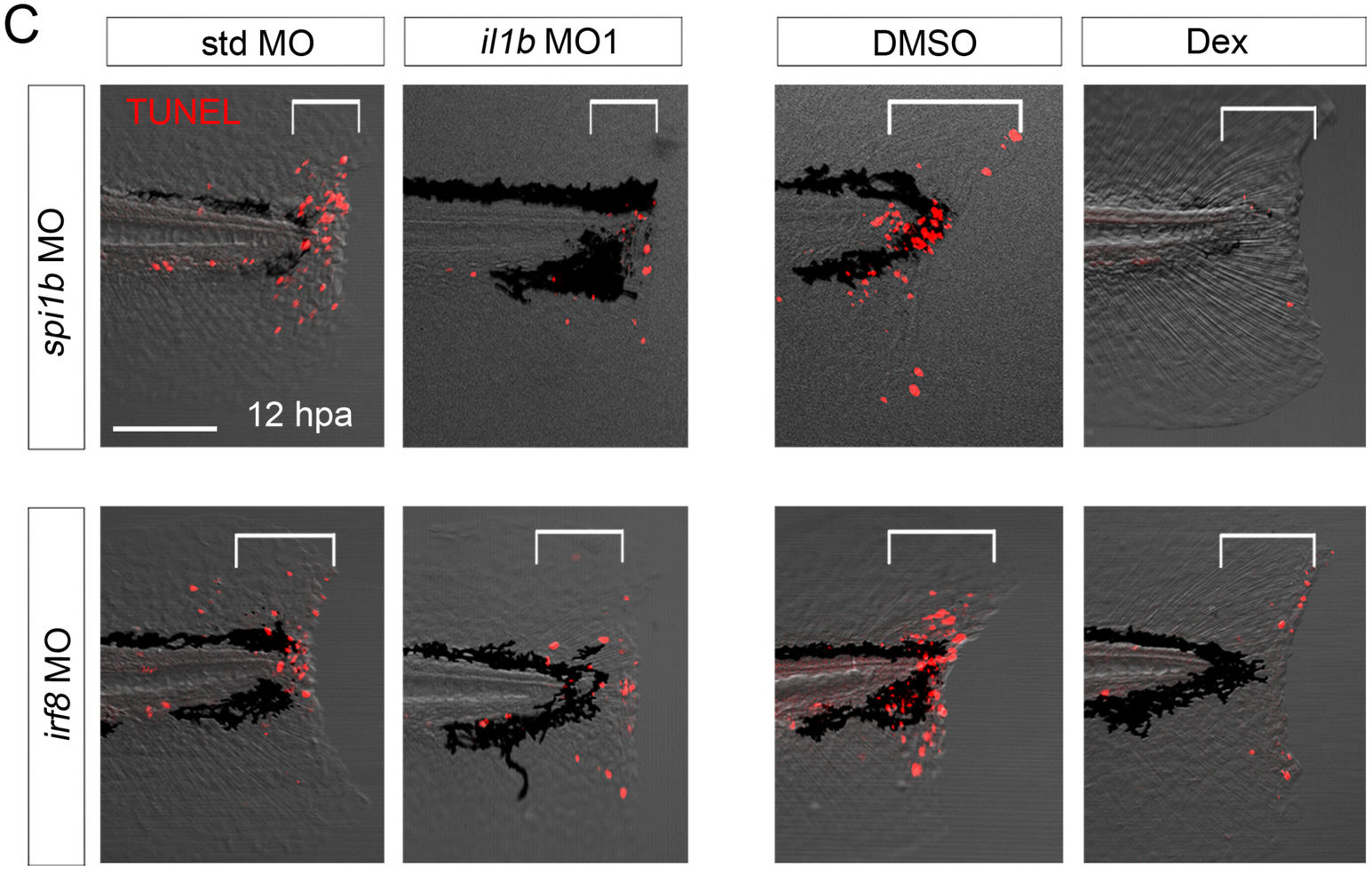
std MO
il1b MO1
DMSO
Dex
spi1b MO
irf8 MO
TUNEL
12 hpa

D

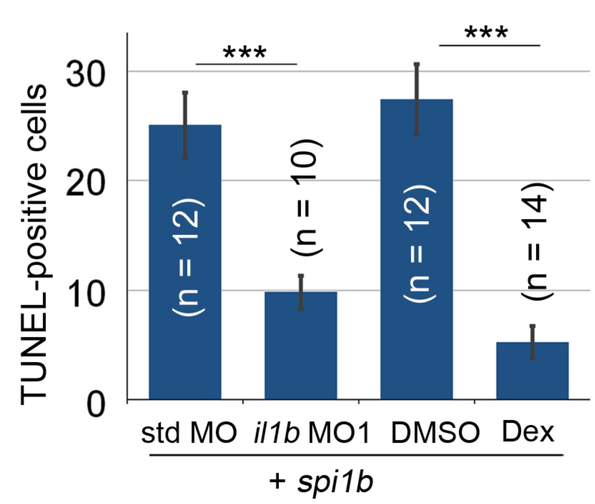
***
***
TUNEL-positive cells
30
20
10
0
(n = 12)
(n = 10)
(n = 12)
(n = 14)
std MO
il1b MO1
DMSO
Dex
+ spi1b

E

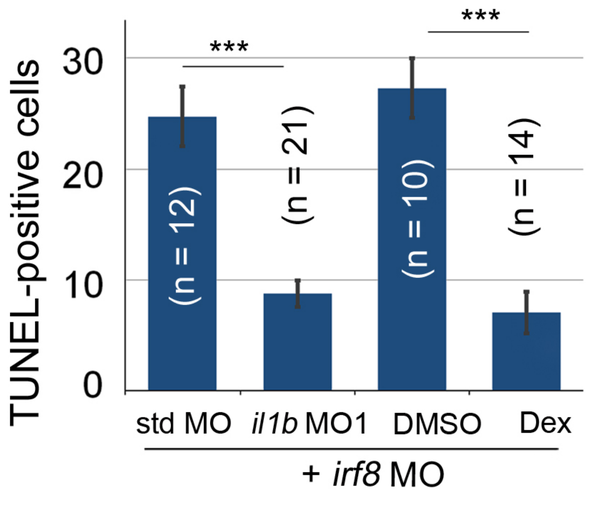
***
***
TUNEL-positive cells
30
20
10
0
(n = 12)
(n = 21)
(n = 10)
(n = 14)
std MO
il1b MO1
DMSO
Dex
+ irf8 MO

A

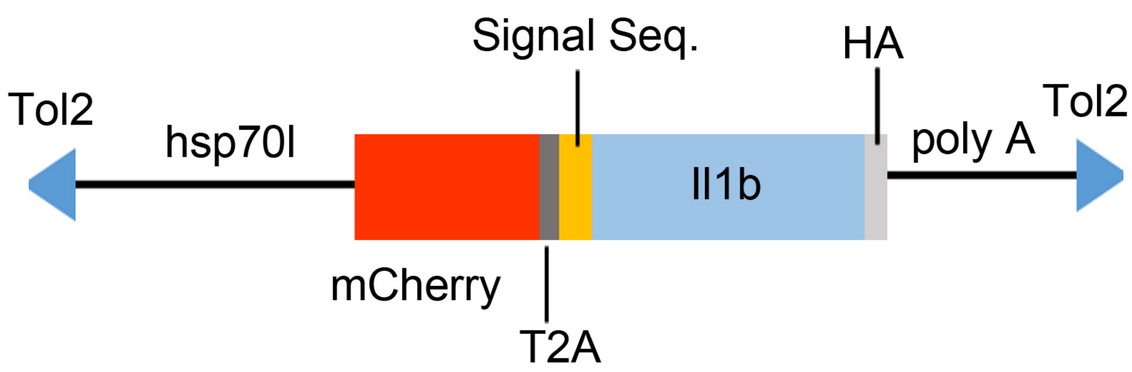
Tol2
hsp70l
Signal Seq.
mCherry
T2A
HA
Il1b
poly A
Tol2

B

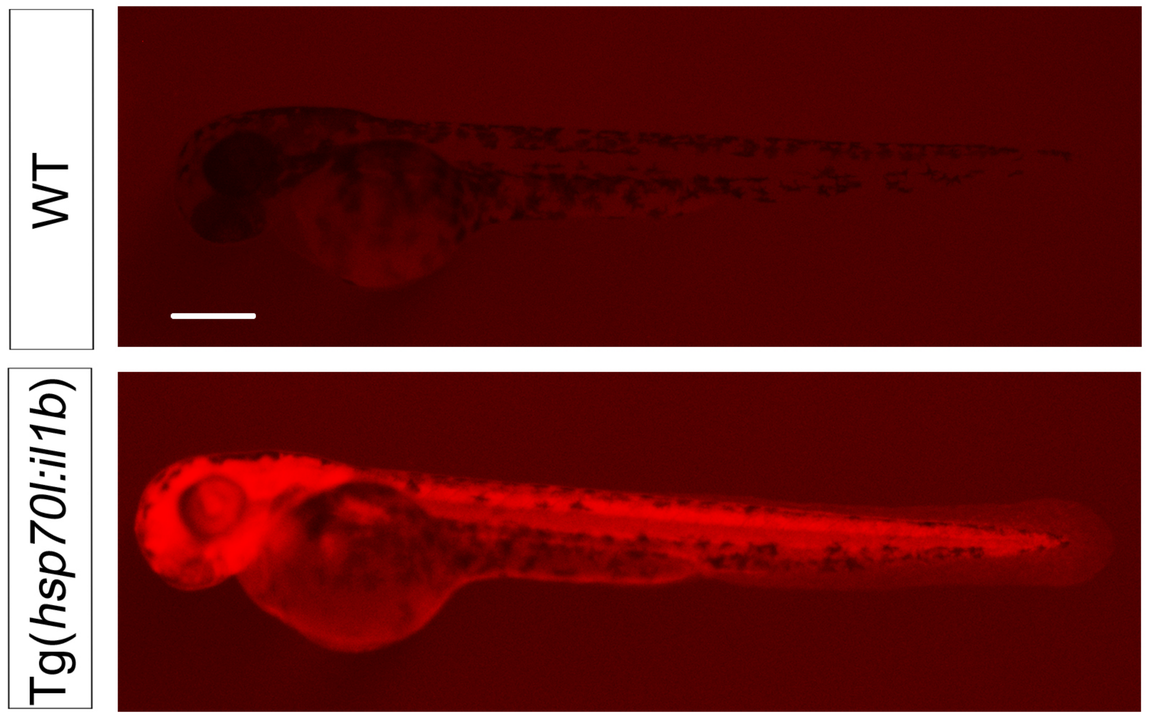
WT
Tg(hsp70l:il1b)
4 hrs after HS

C

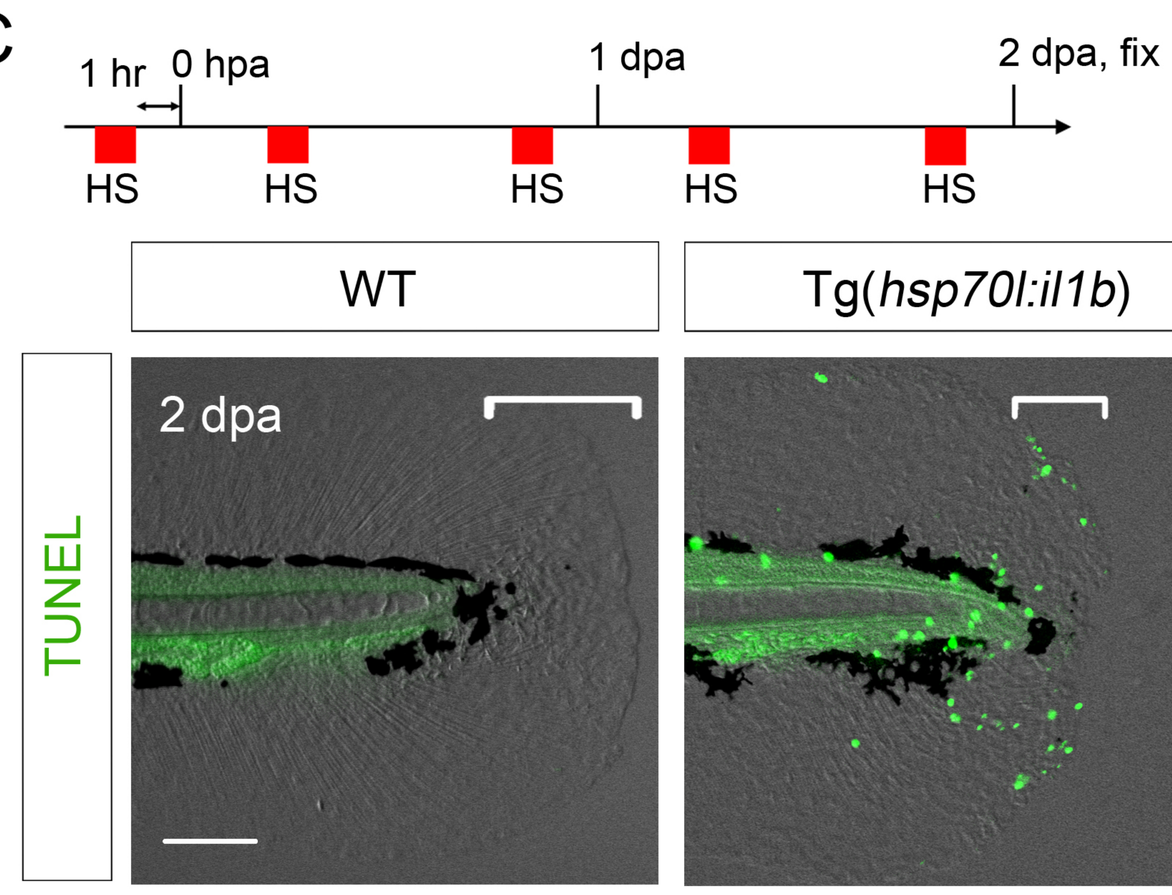
1 hr
0 hpa
1 dpa
2 dpa, fix
HS
HS
HS
HS
HS
WT
Tg(hsp70l:il1b)
TUNEL
2 dpa

D

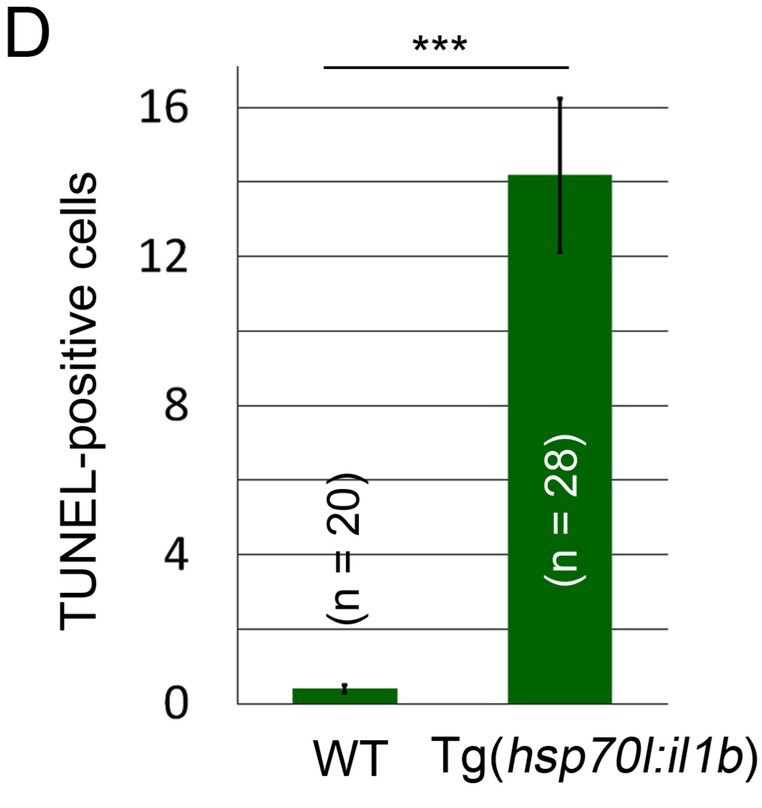
***
TUNEL-positive cells
16
12
8
4
0
(n = 20)
(n = 28)
WT
Tg(hsp70l:il1b)

E

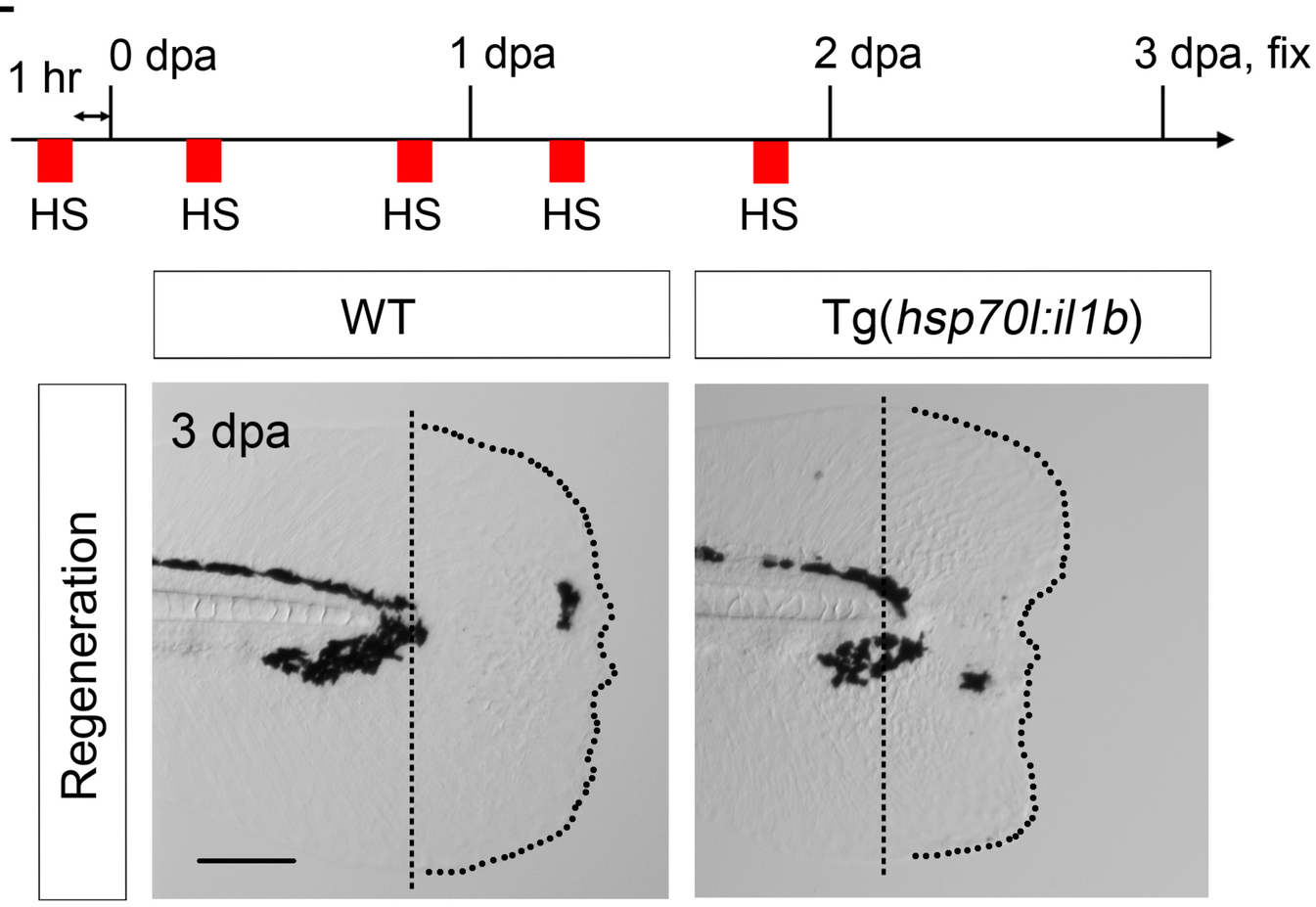
1 hr
0 hpa
1 dpa
2 dpa
3 dpa, fix
HS
HS
HS
HS
HS
WT
Tg(hsp70l:il1b)
Regeneration
3 dpa

F

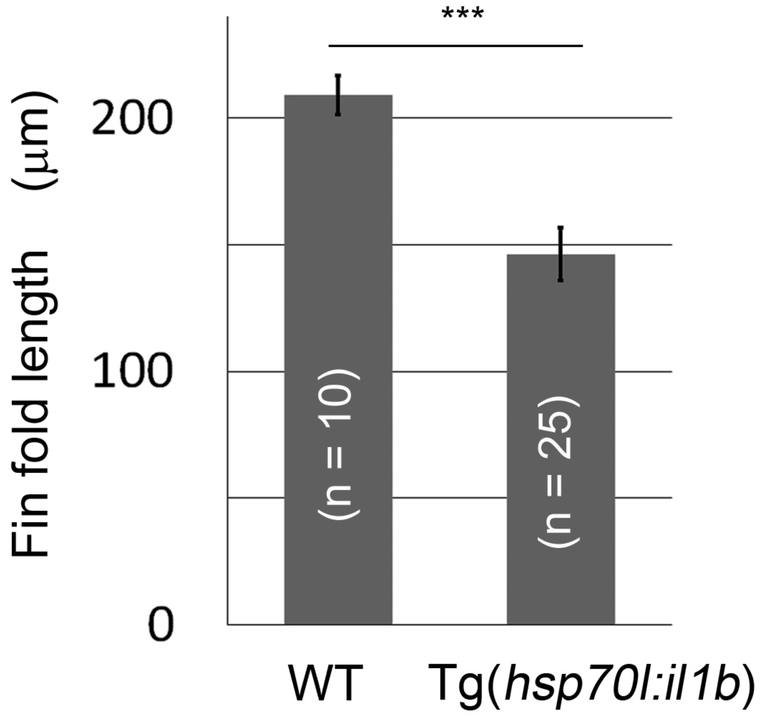
***
Fin fold length (μm)
200
100
0
(n = 10)
(n = 25)
WT
Tg(hsp70l:il1b)

A

Regeneration

DMSO

3 dpa

Dex

B

Fin fold length (μm)

200
150
100
50
0

***

(n = 29)

(n = 32)

DMSO Dex

C

BrdU

DMSO

24 hpa

Dex

D

BrdU-positive cells

60
50
40
30
20
10
0

***

(n = 29)

(n = 37)

DMSO Dex

E

junba *junba* *fgf20a*

DMSO

3 hpa 12/12

12 hpa 19/19

12 hpa 11/11

Dex

10/10

20/24

11/11

F

Regeneration

std MO

3 dpa

il1b MtO1

G

Fin fold length (μm)

200
150
100
50
0

***

(n = 45)

(n = 49)

std MO *il1b* MO1

H

BrdU

std MO

24 hpa

il1b MO1

I

BrdU-positive cells

60
50
40
30
20
10
0

**

(n = 29)

(n = 34)

std MO *il1b* MO1

J

junba *junba* *fgf20a*

Std MO

3 hpa 14/15

12 hpa 12/13

12 hpa 17/18

il1b MO1

12/18

17/17

17/19

K

2 dpf

2.5 dpf, fix

1 hr

1 hr

6 hrs

L

fn1b *junba* *junbb*

WT

22/22

15/15

20/20

Tg(*hsp70l:il1b*)

27/27

20/20

22/22

A Tissue injury

Injury

Epithelial cells

Mesenchyme

B Il1b induction
Priming of regeneration

il1b induction

Il1b

Primed regenerative cells

Expression of
regeneration-induced genes

C Attenuation of Il1b expression
Normal regeneration

il1b

Macrophage-derived
factor

Survival of
regenerative cells

D Absence of macrophage

il1b

Excessive Il1b

Apoptosis

A

Tg(*il1b*:*egfp*)

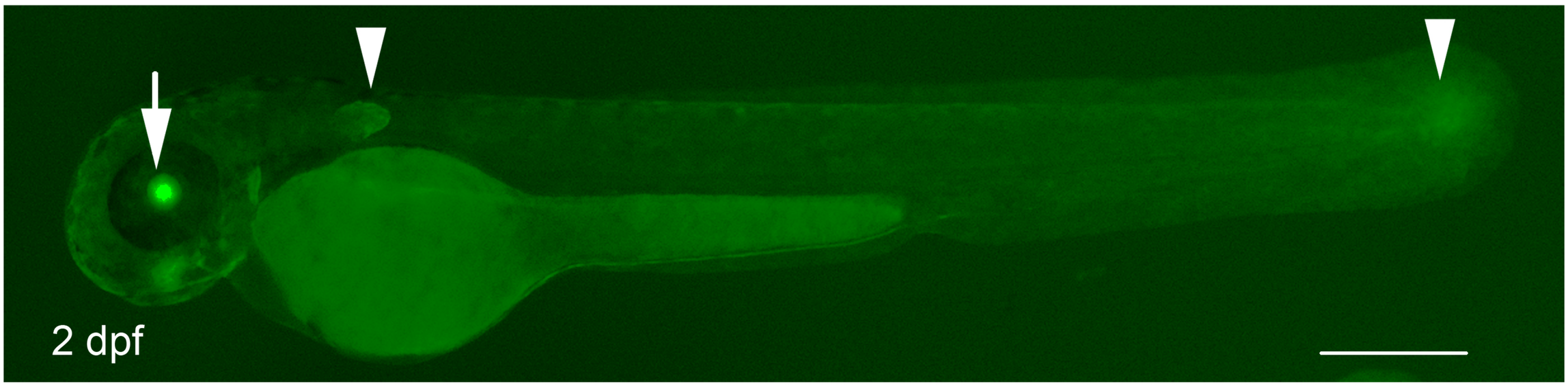

B

3 hpa

Tg(*il1b*:*egfp*)

egfp

il1b

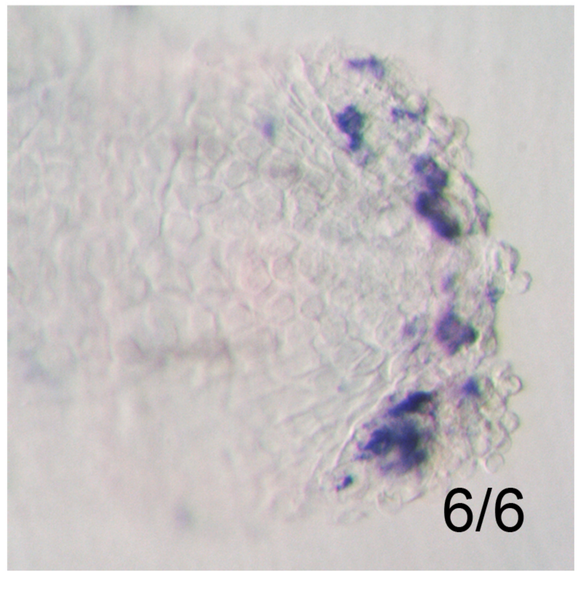

C

Tg(*il1b*:*egfp*)

Phenol Red

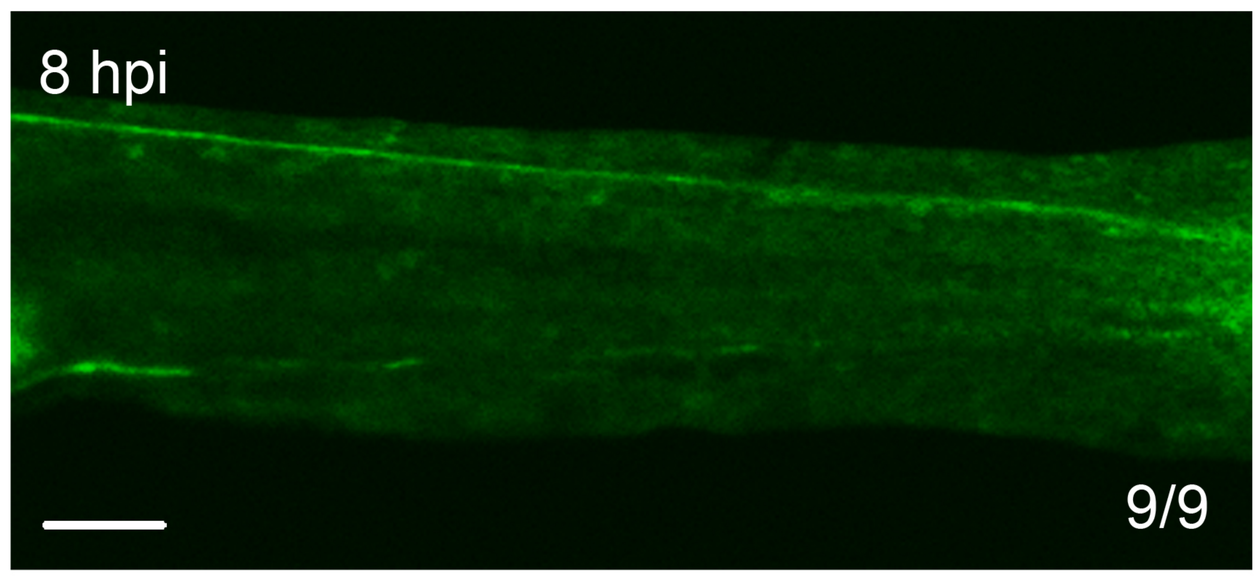

LPS

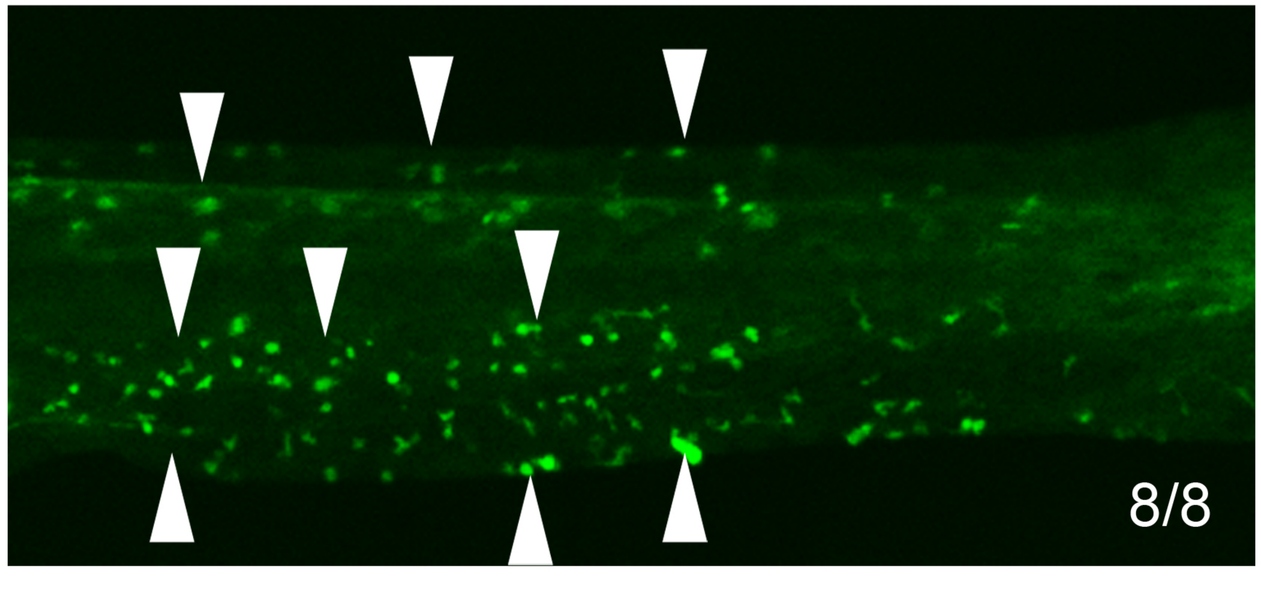

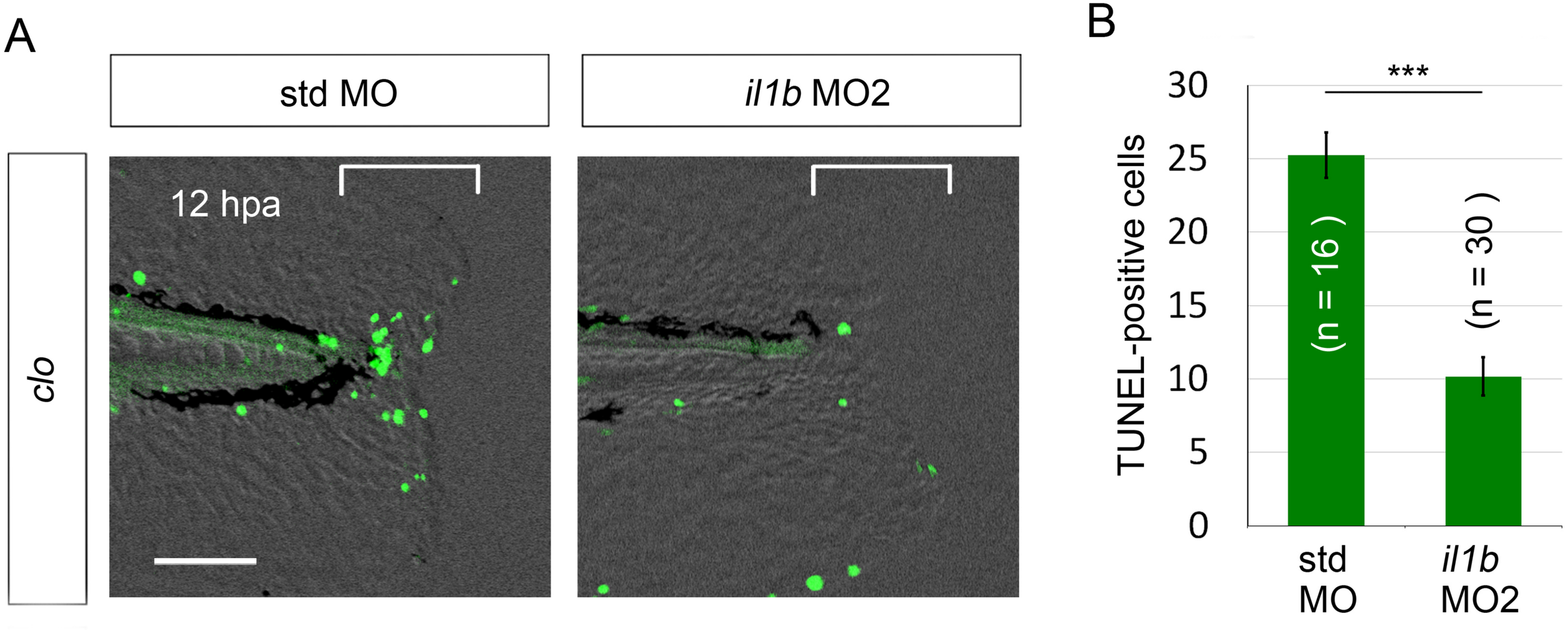
A
std MO
il1b MO2
clo
12 hpa
B
TUNEL-positive cells
30
25
20
15
10
5
0
***
(n = 16)
(n = 30)
std MO
il1b MO2

A

Sudan black staining

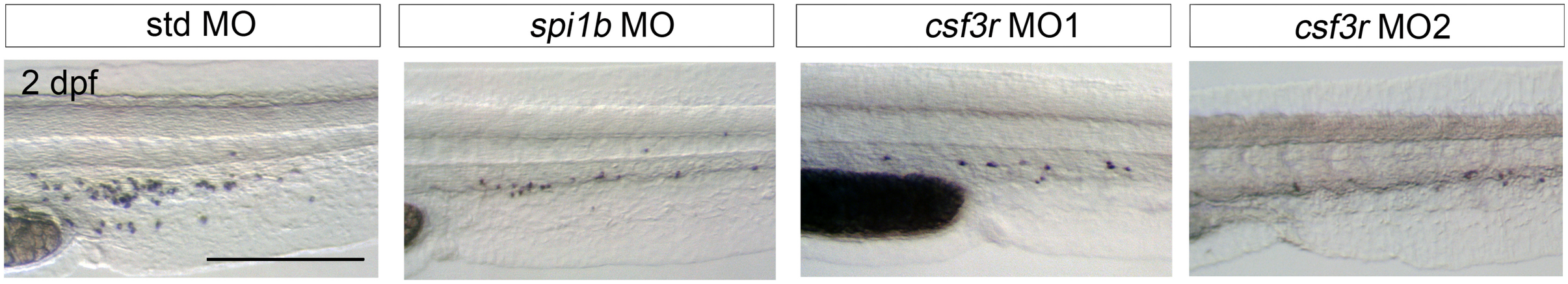

B

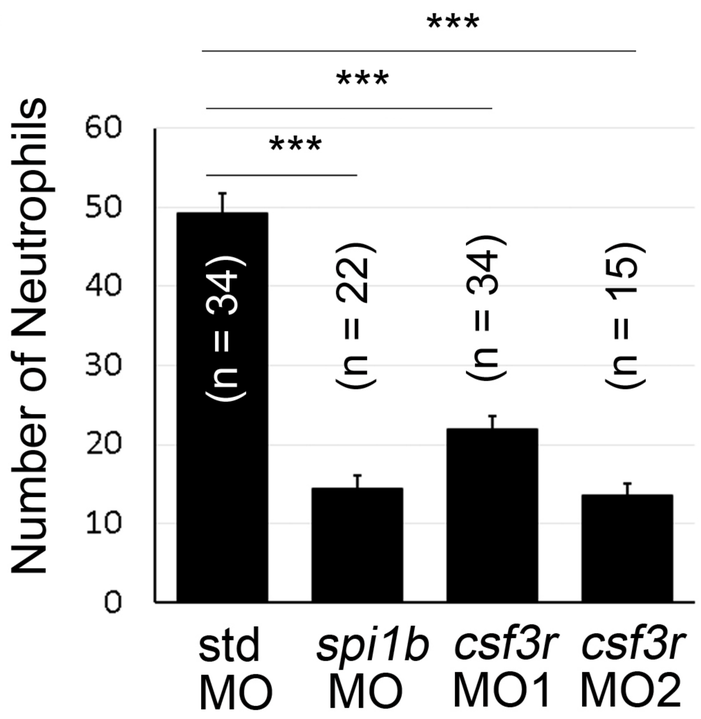

C

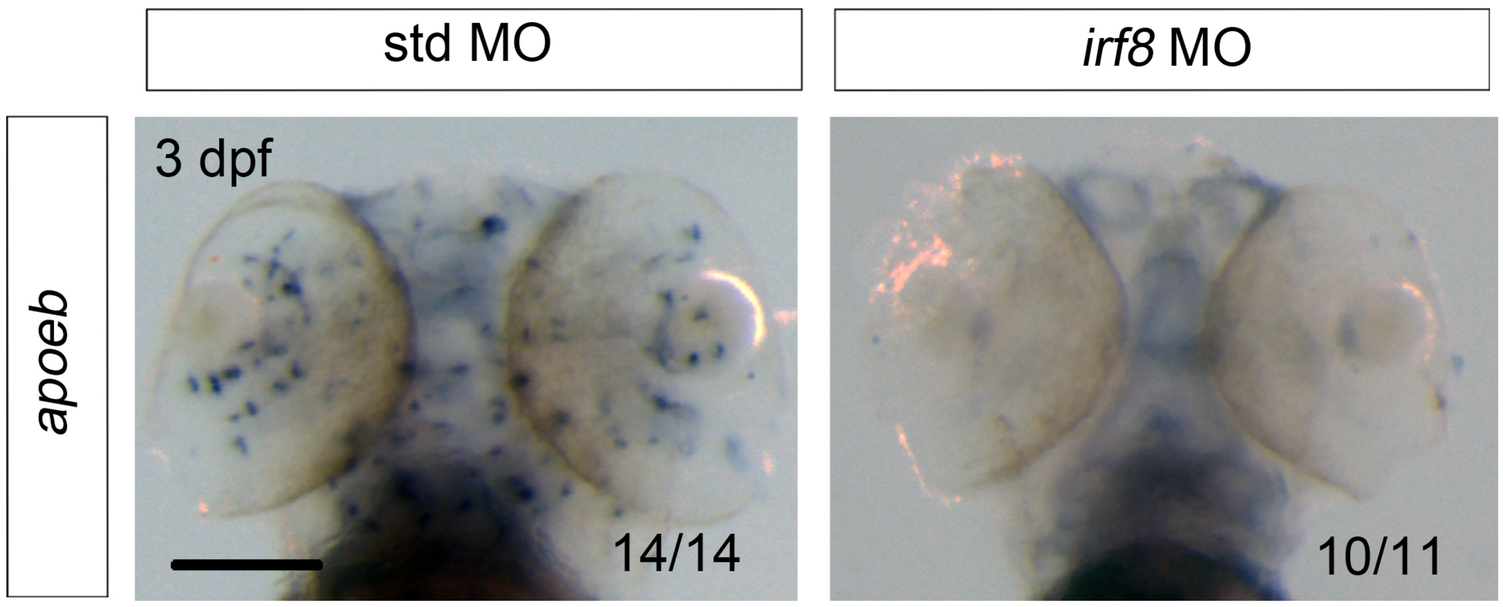

D

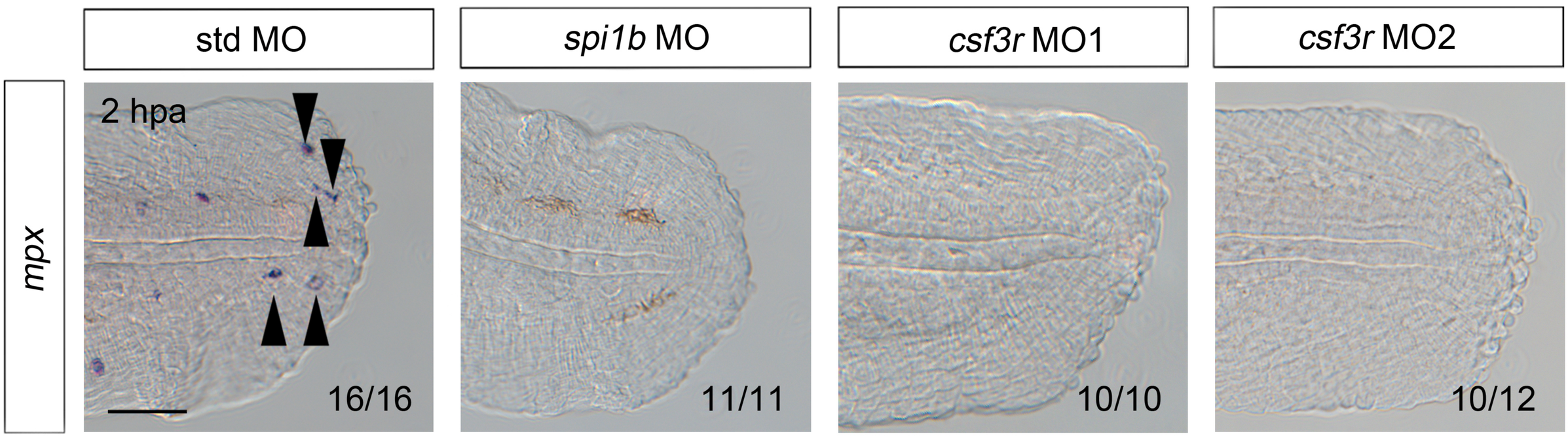

E

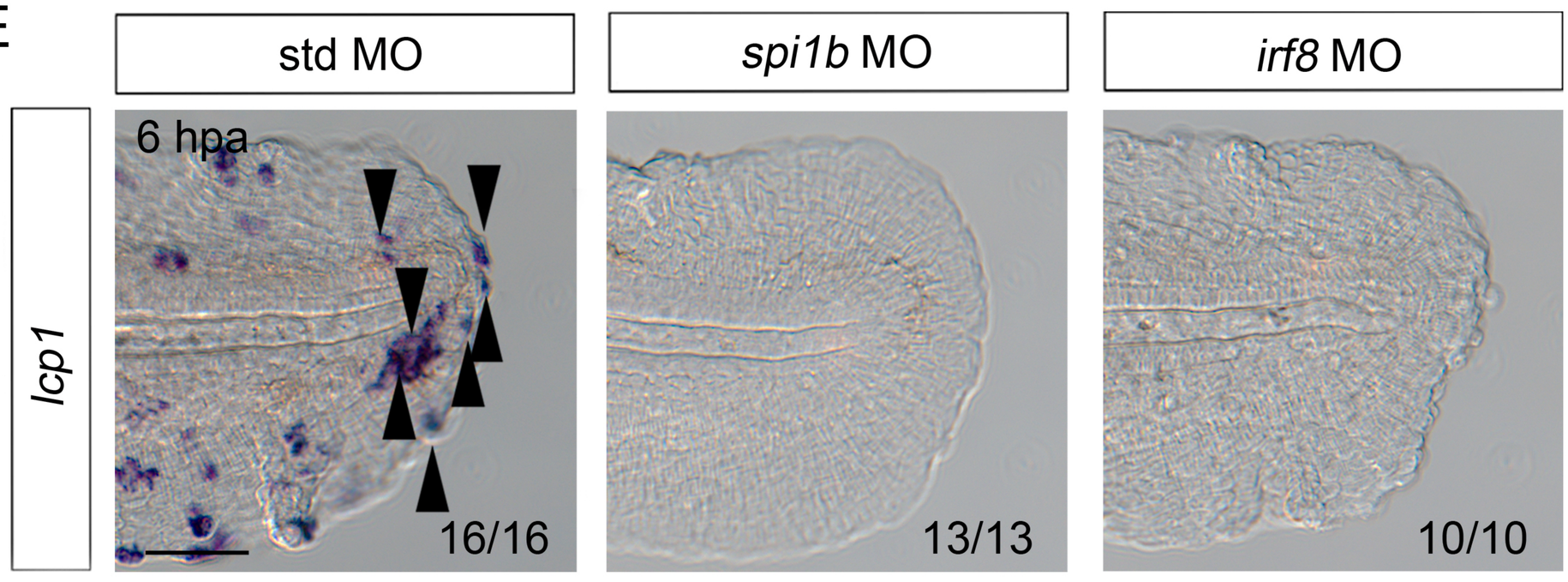

A

Human Il1b cleavage site

```
Human      110:NEAYVHDAPVRSLNCTLRDSQQKSLVMS-GPYELKALHLQGQDMEQQVVFSMS-FV-QGE 166
Zebrafish  118:VPSYTKTKNV--LQCTICDQYKKSLVRSGGSPHLQAVTLRAGSSDLKVRFSMSTYASPSA 175
```

Estimated zebrafish Il1b cleavage site

B

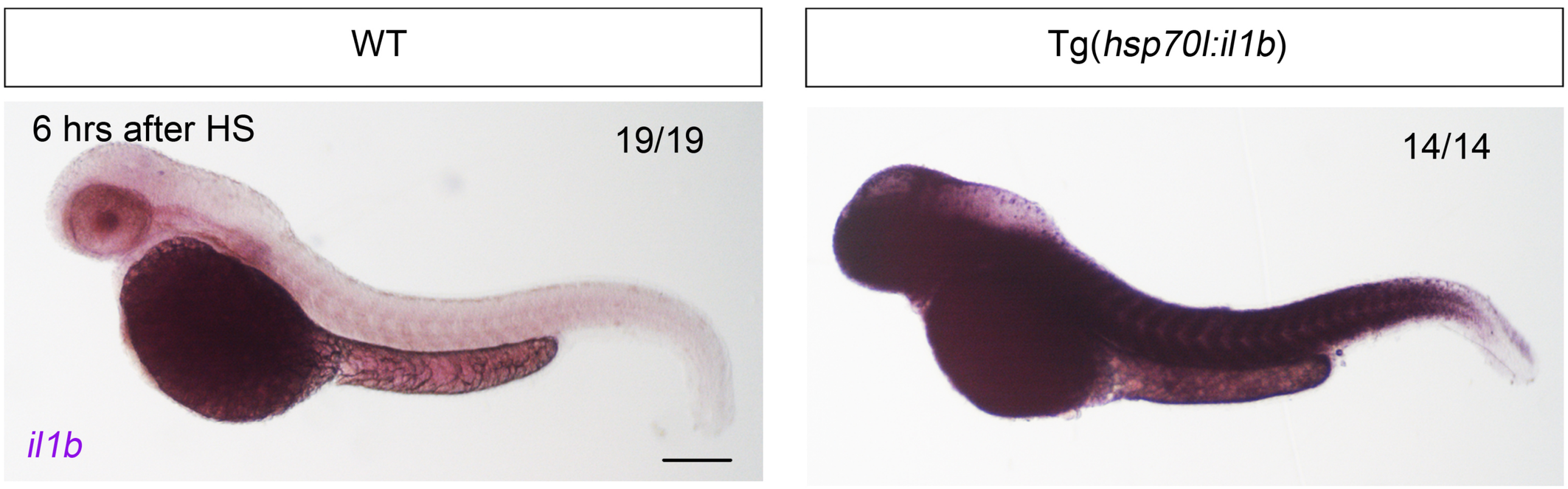

C

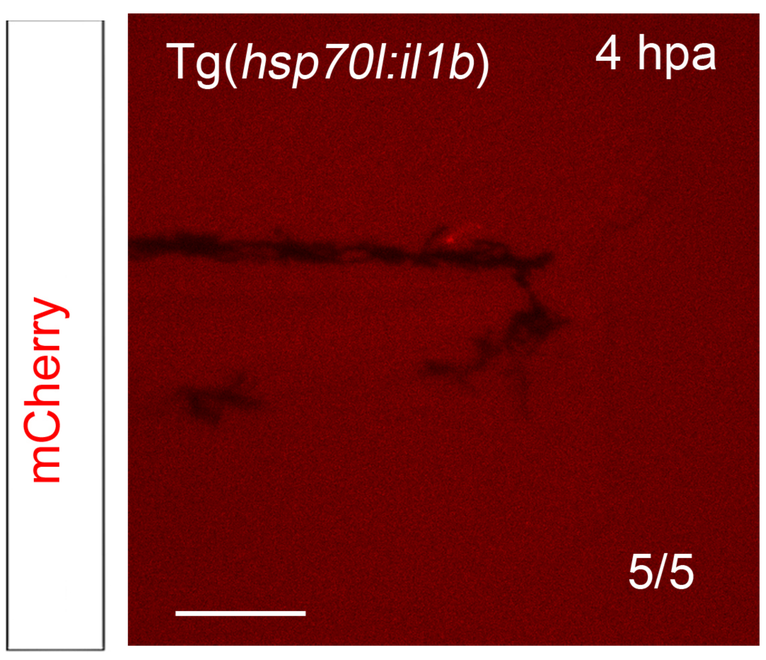

D

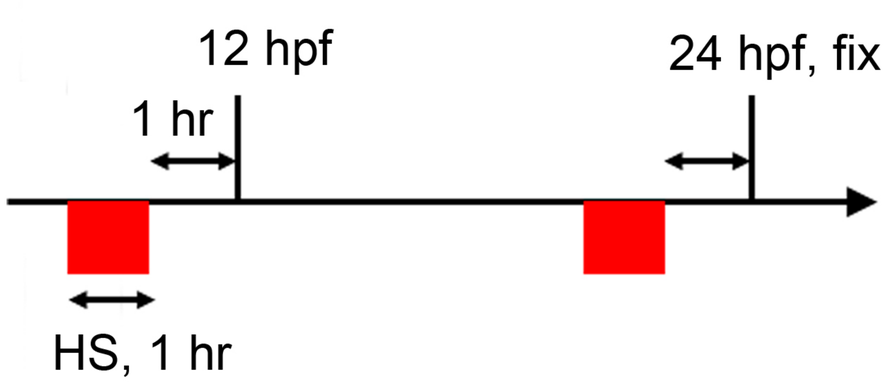

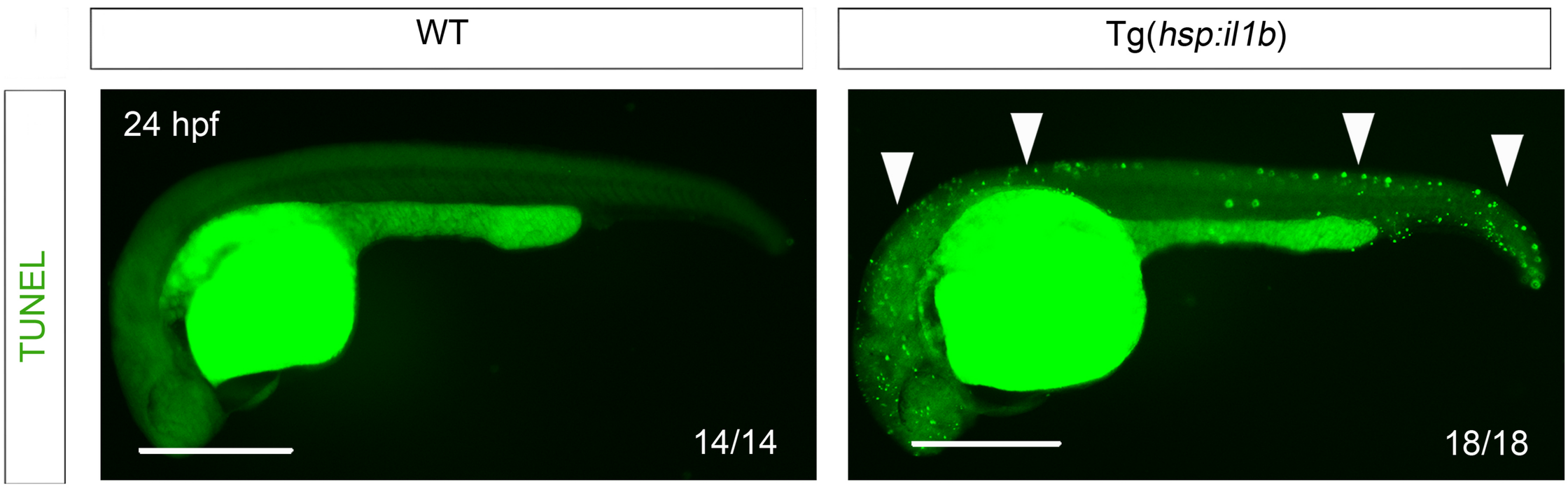

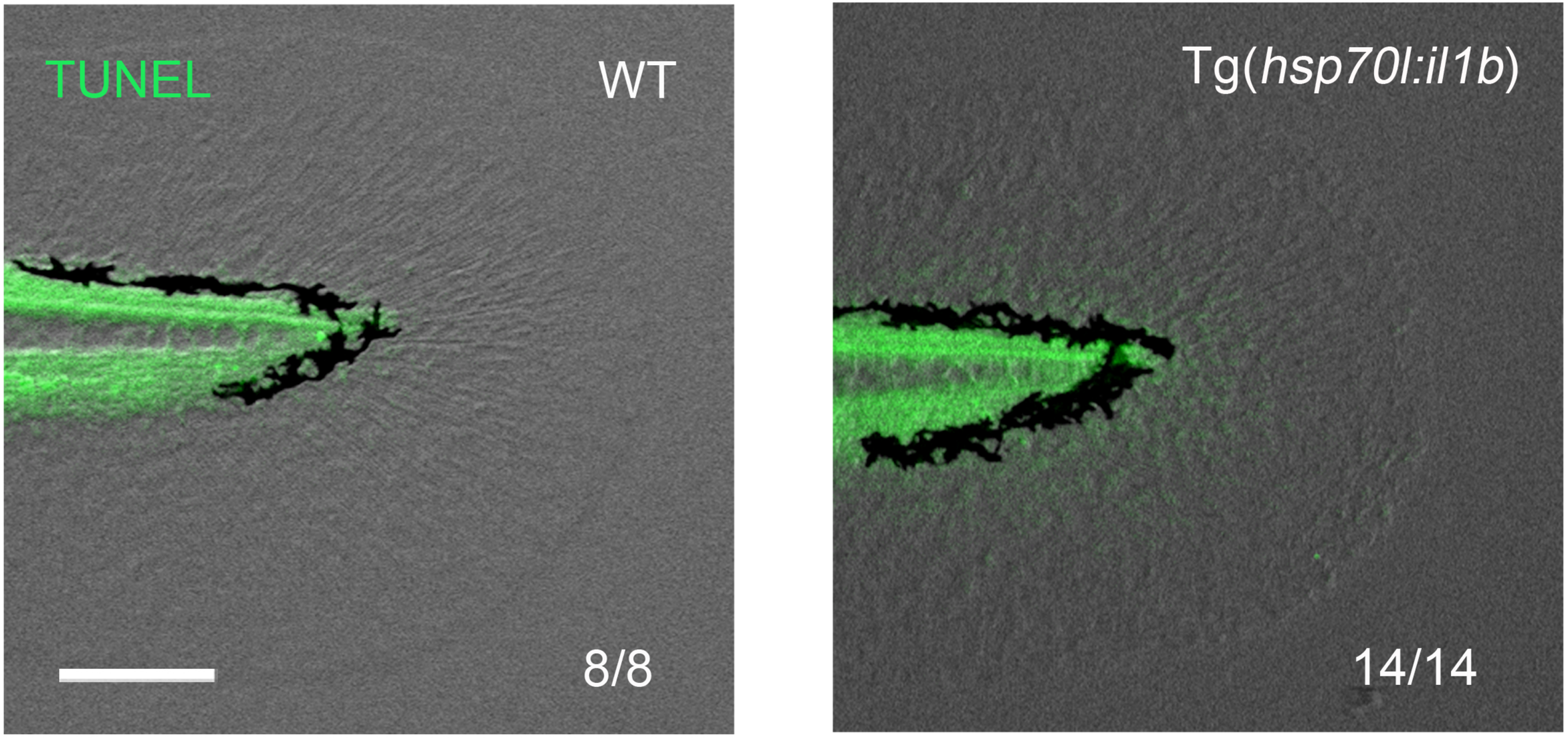
TUNEL
WT
8/8
Tg(*hsp70l:il1b*)
14/14